Sensitivity of the Urban Boundary Layer to Model Parameterization

Joseph E. Wermter

Submitted to the graduate degree program in Department of Geography and Atmospheric Science and the Graduate Faculty of the University of Kansas in partial fulfillment of the requirements for the degree of Master of Science.

David A. Rahn, Ph.D. (Advisor)

Committee Members:

David B. Mechem, Ph.D.

Joshua K. Roundy, Ph.D.

Date Defended: 8/21/2020

The Thesis Committee for Joseph E. Wermter certifies
that this is the approved version of the following thesis:

Sensitivity of the Urban Boundary Layer to Model Paramterizations

David A. Rahn, Ph.D. (Advisor)

Date Approved: 8/21/2020

Abstract

Continued urbanization and a warming climate will exacerbate the urban heat island (UHI) and aggravate health risks of urban populations. In addition to satellite and surface observations, high resolution numerical simulations are often used to study the UHI. Less attention is typically given to the urban boundary layer (UBL) mainly because upper-air observations are sparse or limited to short field campaigns, which also makes verification of model profiles challenging.

The continued growth of observations from the Aircraft Meteorological Data Relay (AMDAR) provides essential measurements of the lower atmosphere, which are collected by many commercial airplanes during landing and takeoff. AMDAR data from airports reasonably close to urban centers yields many profiles of the UBL per day that can be used to evaluate model performance and better understand the lower atmosphere over urban areas. The Weather Research and Forecasting (WRF) modelling system is used to simulate the urban environment of the Dallas-Fort Worth metropolitan area during recent heat waves. Model output is evaluated using AMDAR soundings from two airports (DFW and DAL) to not only assess overall performance but also to help identify specific model deficiencies and highlight the important role of the lower atmosphere in influencing surface temperatures and the magnitude of the urban heat island.

Focus is placed on the interaction of urban canopy model and planetary boundary layer (PBL) schemes. Major differences are found in the lower atmosphere primarily in the morning and evening hours with the most similar profiles during the daytime. Warm biases are often present at the surface in the model and are related to deeper mixing in the model than observed. Morning observations often indicate a shallow mixed layer near the surface capped by a stable layer associated with a temperature inversion or an isothermal layer. Some cases reveal situations where the layer of stability is not captured by the model and the temperatures at the top of the layer are often greater than simulations. This likely represents warmer temperatures that remained confined to the residual layer overnight instead of being mixed out as

the model suggests. However, certain simulations have been able to resolve the features of the nocturnal boundary layer in some cases, albeit the inversion is usually at a lower level or not as well defined as the observation. The relative accuracies of these simulations are usually dependent on which closure scheme they employ. Diurnal evolution of the UBL, especially the morning and evening transitions, is simulated differently depending on the choice of the PBL scheme. Streamwise cross-sectional analyses also confirm that closure schemes are essential in simulating lower atmospheric stability in the urban regions.

Acknowledgements

I would like to thank my advisor, Dr. Dave Rahn, for providing this opportunity to do research at a graduate level, and for serving as a mentor throughout my time at the University of Kansas. I also am grateful for the help and feedback from committee members Dr. Dave Mechem and Dr. Josh Roundy.

Fellow student Tim Cady was extremely helpful as I was establishing myself in this project, and the learning curve would not have been as easy without his technical support. Although they weren't research partners, I would like to thank fellow students Brett Chrisler and Morgan Stessman for a swift welcoming into the department, and for being great friends.

Finally, I am immensely grateful for everything my family has done to support me as I pursued my career in atmospheric science.

Contents

1 Introduction

The Urban Heat Island (UHI) affects a large portion of the human population and essentially describes higher temperatures in urban areas compared to rural areas. Anomalously higher temperatures are a result of drastic changes to the landscape from urban development. UHI effects have been observed for over a century and are the first known direct anthropogenic changes to the weather and climate (Cosgrove & Berkelhammer 2018). UHI intensity depends on the local climate and the physical properties of the built environment, such as surface roughness, albedo, and permeability (Zhao *et al.* 2014). Due to the multitude of processes occurring over various spatial and temporal scales, simulating urban areas remains a challenge, and improving the representation of the UHI in models is an active area of research (Rizwan *et al.* 2008).

Many factors impede progress towards improving numerical simulations of the UHI. A sufficiently small model grid spacing is necessary to adequately resolve the urban area, so substantial computing resources are required. This issue is becoming less of a burden with ever-increasing computing power, but it is still a limitation. Although heterogeneous land cover is also an issue for natural vegetation, it is even a greater issue for complex urban environments that exhibit such a wide range of structures and configurations. So, it is necessary to include the most realistic representation of the urban environment (e.g., building material, building heights, street canyon width). Even with high resolution model grids and an accurate representation of building characteristics, additional atmospheric processes unique to the built environment (e.g., treatment of radiation in street canyons) must be accounted for. Finally, it is vitally important to assess the model output with observations. While this is an obvious step, it is often a challenge over urban areas due to a lack of observations.

Over the last few decades of the 20^{th} century, many studies quantified the local impacts of urbanization with surface-based observations (Changnon *et al.* 1971; Harnack & Landsberg 1975). The representativeness of surface observations within urban areas can be questionable since the microclimates can exert such a great influence on the point measurements. By using

satellite-derived temperatures over an urban area, the spatial distribution can be readily found (Sobrino *et al.* 2013), however there are issues such as cloud cover obscuring the surface, infrequent temporal sampling of the highest-resolution satellites, and temperature retrieval errors.

While the UHI describes the near-surface temperature anomalies, the vertical component must also be considered. The temperature structure above the urban area is important for the dispersion of pollutants originating from the surface. UHI effects are regarded as part of and as a contributing factor to the characteristics of the Urban Boundary Layer (UBL), which is an important component for understanding the urban environment as a whole (Barlow 2014). Until recently, observations of the UBL have been limited to dedicated field campaigns or operational soundings normally launched twice a day at 0000 and 1200 UTC. With the exponential increase (excluding during the 2020 pandemic) of measurements from commercial aircraft via the Aircraft Meteorological Data Relay (AMDAR), it is now possible to conduct a more rigorous model assessment of the lower atmosphere.

The central goal of this work is to use AMDAR to assess numerical simulations of the urban environment by asking a fundamental question: What are the roles of the surface parameterizations versus the role of the turbulence schemes when determining the errors in the temperatures over an urban area? While these are coupled within the model, a strong sensitivity to one over the other will indicate which is dominant. Using the available observations and running numerical simulations, this question will be addressed in several ways considering both local and non-local sources of errors. A review of the pertinent atmospheric processes is provided in the next section, followed by a description of the numerical simulations and observations. A series of sensitivity runs from the model are compared with each other and the surface and AMDAR observations to assess several aspects of the model output. In the final section, results are summarized and several main conclusions are highlighted.

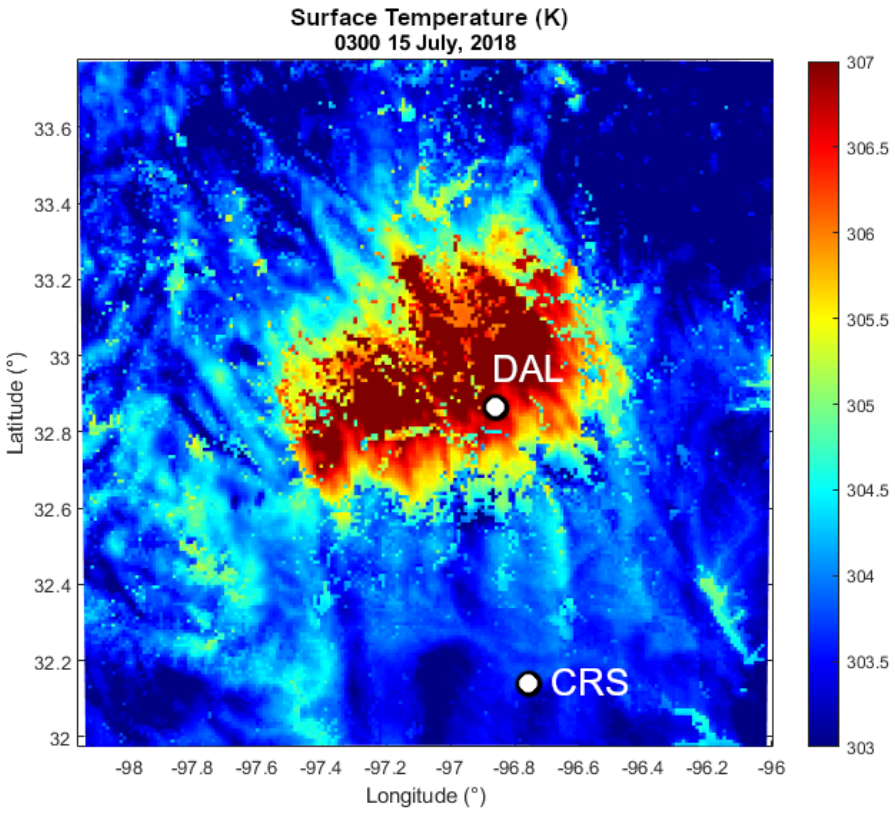

Figure 1: The 2-m air temperature (K) from WRF over the Dallas/Fort Worth metropolitan at 0300 UTC 15 July 2018.

2 Background

2.1 UHI & UBL

The UHI has been studied for the better part of a century (Clarke 1969; Godowitch *et al.* 1985). Urbanization replaces natural land cover with low-albedo impervious surfaces and drastically alters the local radiative balance and energy exchange by reducing evapotranspiration and increasing sensible heat flux (Oke 1988; Arnfield 2003). This results in positive land surface and air temperature anomalies when compared to the rural surroundings (Fig. 1). UHIs are enhanced by anthropogenic processes, most notably from the use of air conditioning systems, emissions from vehicles, and industrial activity (Shahmohamadi *et al.* 2011; Salamanca *et al.* 2014). The UHI and its connection to the mixed-layer depth are related to health risks

associated with heat stress and the concentration of air pollution. Since urbanization and anthropogenic global warming will increase over the next several decades and present numerous threats to health and sustainability, it is crucial to understand the characteristics and behavior of the surface and lower atmosphere over urban areas.

One of the more fascinating aspects of the UBL is the nocturnal evolution compared to the rural boundary layer. In many cases, the development of the typical nocturnal inversion is less pronounced in urban profiles than it is in rural profiles given the warmer surface over urban areas that promotes more mixing over the urban areas than over rural areas where the lower atmosphere tends to stabilize faster (Godowitch *et al.* 1985; Baklanov 2002). Downwind effects of the UBL can also include an "urban plume", which occurs when a secondary rural boundary layer forms downwind of the urban center. Plumes are indicated by higher than normal temperatures and nearly adiabatic profiles between the urban boundary and the secondary rural boundary.

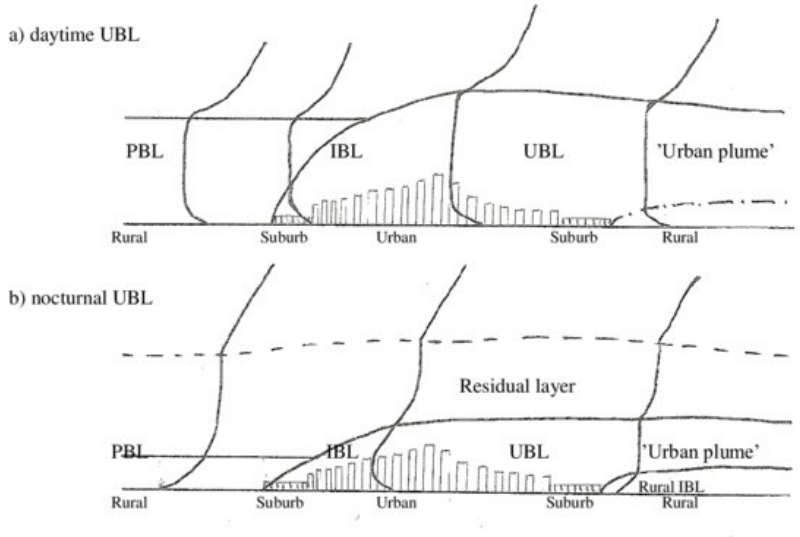

Figure 2: Comparison of daytime and nocturnal UBL schemes, with an illustration of the downwind "urban plume" effect. (Baklanov 2002)

2.2 Numerical Simulations

Advances in computational capabilities permit the UHI to be simulated with high-resolution numerical weather models. This is possible due to the development of sophisticated urban parameterization schemes and high resolution mapping of urban characteristics that are incorporated into models such as the Weather Research and Forecasting (WRF) modelling system (Skamarock *et al.* 2019). WRF has several options to represent subgridscale processes necessary to simulate the atmosphere over urban areas. There are two parameterizations in particular that this project will focus on. The urban canopy model (UCM) represents processes associated with urban areas. The other critical parameterization is for subgridscale turbulence, which is handled by the planetary boundary layer (PBL) scheme. Since the UCM and PBL schemes are of particular importance, some of their details are described below.

2.2.1 UCMs

A UCM requires information on the built environment, which includes many parameters such as building material, building heights, and street canyon width. These properties are ingested from the National Urban Data and Access Portal Tool (NUDAPT, Glotfelty *et al.* 2013). Using these characteristics of the built environment, the UCM accounts for a wide range of processes associated with the urban area, and there are two UCMs integrated into WRF. The Single-Layer Urban Canopy Model (SLUCM), which is simplified geometrically to a "street canyon" design in a single column. The SLUCM calculates variables from the "road surface" at ground level, the "roof surface" at a fixed level "z", and the "wall surface" at the vertical boundary between the surface and "z" (Kusaka *et al.* 2001). SLUCM also considers shadowing, reflection, and radiative trapping in the street canyon (Salamanca *et al.* 2011). Although it is the simplest of the schemes, SLUCM does account for anthropogenic sources of heat flux due to factors such as air conditioning and transportation using a look-up table (Sharma *et al.* 2017).

More precise representation of the urban surface can be attained through a multi-layer UCM. Unlike SLUCM, multi-layer schemes divide the buildings bounding the urban canyon

into several vertical layers. The advantages of a multi-layer scheme include the ability to discretely parameterize buildings of different heights, as opposed to a standard height of the urban canyon that is defined in the SLUCM. Parameterizing a more discrete urban surface is helpful when evaluating turbulence and other mesoscale effects that are the result of the city.

A more sophisticated UCM that uses multiple levels is the Building Effect Parameterization (BEP) scheme, which uses more detailed building information that allows varying heights as a "three-dimensional urban surface." Similar to SLUCM, BEP considers radiative transfer between streets, walls, and rooftops. The BEP scheme accounts for how the three-dimensional urban surface impacts the atmospheric momentum in a more detailed manner than the simplified geometry of SLUCM. BEP does not explicitly consider anthropogenic heating, so an additional scheme was developed to couple with BEP and includes those effects. The Building Energy Model (BEM) accounts for additional factors that improve the BEP scheme (Salamanca & Martilli 2009). The BEP+BEM coupled scheme considers heat diffusion through boundaries such as floors, walls, and roofs of buildings as well as radiative exchange through windows. BEP+BEM also parameterizes anthropogenic factors such as heat generation of building occupants, as well as the radiative effects of air conditioning and building ventilation. These equations rely on the coupling of the BEM and the BEP. The UCM gives values of outdoor air temperature, humidity, and radiation reaching the exterior of the building, which the BEM uses to calculate radiative transfer from exterior to interior as well as the wall and roof temperatures; the BEM returns those values to the UCM. Combined, the UCM and BEM provides estimates for heat fluxes within urban entities that are more accurate than what the UCM can singularly provide. (Salamanca *et al.* 2011; Salamanca & Martilli 2009).

2.2.2 PBL schemes

Multiple PBL schemes are available, but the two schemes analyzed in this study are the Bougeault & Lacarrere scheme (BouLac) and the modified Janjić 1990 scheme (MYJ) since these closure schemes are the only ones both coupled to the SLUCM and also the BEP+BEM urban

canopy schemes (Skamarock *et al.* 2019). Above the UCM, the ability of the model to represent turbulent transport is essential to the structure of the lower atmosphere and the surface temperature. Sub-grid scale fluxes are represented by the Reynolds stress terms, and in WRF it is handled by the PBL parameterization.

How to formulate the turbulence is not a trivial problem since the sub-grid scale flux terms always have more unknowns than knowns, so the system can never be "closed" and leads to the well-known closure problem. At some level, an approximation must be made with known variables. There are several ways to approach the closure problem including local (unknowns related to model variables at or adjacent to a grid point) and non-local (unknowns related to model variables anywhere on grid) parameterizations. The methodology behind many PBL schemes is fundamentally influenced by eddy diffusivity (K-theory) which assumes that there is a down-gradient flux for any conserved variable (e.g., potential temperature (θ), mixing ratio) and is analogous to molecular diffusion such that

$$\overline{w'\theta'} = -K\frac{\partial\overline{\theta}}{\partial z} \tag{1}$$

where the flux is proportional to the gradient of the mean variables and an "eddy diffusivity" for that variable, which is represented by K. In the most elementary form of this flux-gradient method, the value of K is constant and can be empirically estimated. Values of K can be explicitly prescribed as a fixed shape of a typical profile that uses surface layer similarity theory and is scaled to boundary layer height resulting in a non-local scheme (e.g., O'Brien 1970); however, implicit estimations of K are normally preferred. General formulations of K above the surface layer are often expressed as functions of the parcel mixing length scale (l) and Richardson Number (Ri) that represents wind shear and stability such that (Arya 2001):

$$K = l^2 * |\frac{\partial\vec{v}}{\partial z}| * f(Ri) \tag{2}$$

In this case, $f(Ri)$ is an emperical function of the bulk Richardson Number. There are numer-

ous ways to formulate $f(Ri)$, and the parameterization is often separated into a stable and an unstable stratification regime. Both the MYJ and BouLac take a more sophisticated approach by estimating the diffusivity using a prognostic turbulent kinetic energy (TKE) equation.

In well-mixed layers of the atmosphere, a fundamental issue arises in Eq. 1. Given a well-mixed profile of a daytime convective boundary layer, there can be no local gradient of average potential temperature (θ) in the middle of the layer even though there are convective thermals that can extend throughout the entire depth of the boundary layer that are associated with heat flux. To deal with the formulation that turbulence always occurs down-gradient, some PBL schemes include an extra term in just the convective PBL to allow for slightly stable stratification to persist with upward heat flux at the top of this layer:

$$\overline{w'\theta'} = \begin{cases} -K\frac{\partial\theta}{\partial z}\text{ , elsewhere} \\ -K(\frac{\partial\theta}{\partial z}-\gamma)\text{ , convective PBL} \end{cases} \tag{3}$$

where γ is the counter-gradient correction term on the order of 0.7×10^{-3} K m^{-2} (Deardorff 1972), which essentially parameterizes non-local effects.

Higher-order turbulence closures presume that if a crude assumption of second moments predicts first moments adequately, then a crude assumption of third moments should predict second moments adequately (Lumley & Khajeh-Nouri 1974). The idea is that if higher order equations are solved, then the model should perform better. Higher-order equations can be derived from the equations of motion, temperature, or moisture fluctuations with additional assumptions such as horizontal homogeneity so that the horizontal fluxes are neglected.

The two PBL schemes in WRF that are integrated with both SLUCM and the multi-level canopy models of BEP and BEP+BEM are MYJ (Mellor & Yamada 1982; Janjić 1990) and BouLac (Bougeault & Lacarrere 1989). Both of these schemes, as implemented in WRF, are considered local 1.5-order parameterization schemes that are based on a prognostic equation for TKE that can be used to improve the parameterizations for the eddy diffusivity (K). In the BouLac

scheme, second-order moments in the prognostic TKE equations are parameterized similarly to Eqs. 1 and 3 using a constant counter-gradient in the heat flux as suggested by Deardorff (1972). The eddy diffusivities for heat, momentum, and TKE are identical with the diffusion coefficients related to the TKE by:

$$K = C * l * \sqrt{\text{TKE}} \tag{4}$$

where C is a coefficient and l is a characteristic length scale for the eddies. The characteristic length scale is related to the distance a displaced parcel can travel and formulated in such a way as to allow for remote effects of stable zones to influence the value. The formulation is similar to MYJ, but C and l are treated separately and are not identical for different types of fluxes (e.g. heat, momentum, and mass) as in the BouLac formulation, which essentially uses information related to the Richardson number (wind shear and stability) to determine the length scale and the coefficients.

3 Data and Methodology

3.1 Study Area and Observations

The primary focus of the study is the metropolitan area of Dallas and Fort Worth because it is a major urban area prone to heat waves, away from any coastal influence, and has ample AMDAR observations. Dallas Love Field (DAL) is located near the center of the Dallas UHI and Dallas/Fort Worth International Airport (DFW) is roughly in between the urban centers of Dallas and Fort Worth, but still strongly influenced by the UHI generated by the two metropolitan regions.

While dedicated studies and field campaigns have provided invaluable knowledge of the UBL, the data used in such endeavors are either not frequent enough or not expansive enough. AMDAR is a useful resource for providing many vertical soundings with high temporal frequencies of at least several an hour at major airports around the world. The data is collected by me-

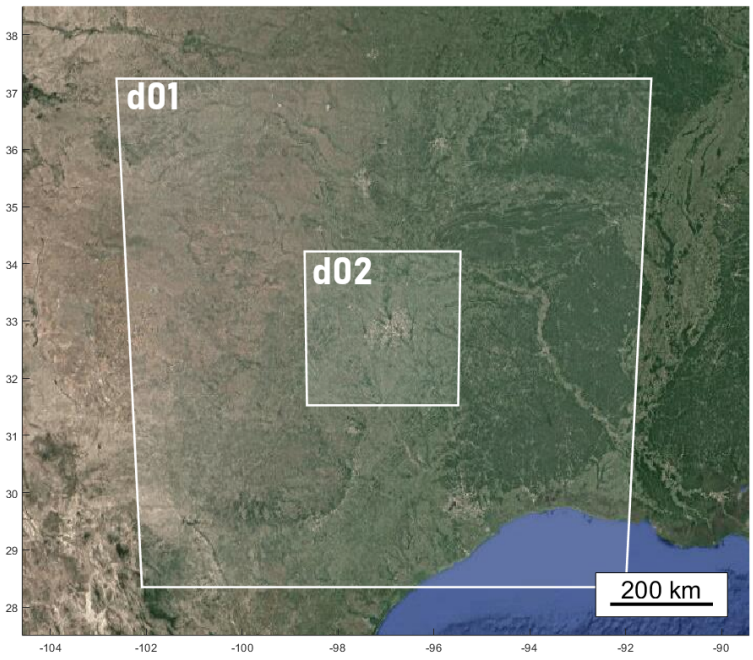

Figure 3: Outer (d01) and inner (d02) domains used in WRF

teorological instruments mounted onboard commercial aircraft that record temperature, pressure, and sometimes humidity, which is then transmitted to data centers in real time. Soundings of the lower atmosphere near airports can be created using the data collected as aircraft land and takeoff following the methods of Rahn & Mitchell (2016). With aircraft frequently arriving and departing at major airports within or near urban centers, the data that the AMDAR instruments provide can help build a solid base of observations that can be used to examine and verify model output. Given the nonuniform nature of aircraft departures and vertical profiles used, all of the profiles are grouped into hourly bins and then that data is interpolated to a single sounding with 20-meter height intervals to give 24 profiles for each day.

3.2 WRF Base Configuration

For each period and sensitivity run, WRF is initialized with the National Centers for Environmental Prediction's North American Mesoscale Forecast System (NAM) analysis. The outer

Table 1: List of base parameterization schemes in WRF

Parameterization	Option	Reference
Microphysics	WSM3 Simple Ice Scheme	Hong *et al.* 2004
Shortwave Radiation	RRTMG	Iacono *et al.* 2008
Longwave Radiation	RRTMG	Iacono *et al.* 2008
Cumulus	Kain-Fritsch	Kain & Fritsch 1993
Land Surface	Noah MP	Niu *et al.* 2011

domain has a 1000 km x 1000 km grid size with a 5 km grid spacing, and the nested inner domain has a grid size of 301km x 301km with a grid spacing of 1 km (Fig. 3). Other parameterizations within WRF are kept constant and are listed in Table 1. Detailed information on the built environment (i.e., building height distributions, street canyon width, building material, and so on) are obtained from the National Urban Data and Access Portal Tool (NUDAPT) (Glotfelty *et al.* 2013).

3.3 Mixed Layer Height Estimations

Depth of the mixed layer is an important parameter to diagnose differences in model performance, so an objective method to quantify the height must be established. Representative measures of mixed layer depth is a concept that is continually discussed, and there are different philosophies towards calculating the depth depending on what observing system is being used or how numerical simulations are formulated. The value for PBL height that is output in a WRF simulation is dependent on which PBL closure scheme is being used. Each of the PBL schemes used in this study are "local" mixing schemes, and as such are sensitive to high-frequency TKE fluctuations with only extremely large eddies at the 1-km grid scale. Estimations of PBL depth tend to be the best during the daytime when the PBL is well-mixed, but previous studies have suggested that they are highly inconsistent with observations during the morning transition (LeMone *et al.* 2013). Under nocturnal conditions, the estimates aren't as variable, but verification to the observations is an issue regardless of the time of day. The Bulk Richardson Number

(Ri_b) method is often used as a simple but robust method to estimate mixed layer heights (Seidel *et al.* 2012):

$$\mathrm{Ri}_b(z) = \frac{g}{\theta(z_0)} \frac{[\theta(z) - \theta(z_0)][z - z_0]}{u(z)^2 + v(z)^2}$$

where g is the gravitational constant (9.81 $\frac{m}{s^2}$), z is the current height level, z_0 is the intial model level, θ is potential temperature, and u and v are the zonal and meriodinal winds. The mixed layer height is the height where the Ri_b passes the critical value (Ri_c) of 0.25.

Compared to methods for detecting temperature inversions in the soundings, the Ri_B method produces similar results in the overnight hours, but is more consistent during the morning transition and the evening transition. Thermally-derived PBL methods can have issues during the day when there is no clear capping temperature inversion. Humidity could also be used to help identify the PBL, but humidity measurements are not as common and less reliable in the current AMDAR data set. The evening and morning transitions are essential focal points to the study, so the more consistent Ri_b-derived PBL heights are used in the comparisons.

4 WRF Simulation Overview

For the purpose of the study, a heat wave case of mid-July 2018 is used as the central case study. During this period, there were multiple consecutive days of abnormally hot temperatures for much of the central United States, including the Dallas/Fort Worth area. The two-week period of 14-28 July 2018 is selected since no major disruptions occurred. Simulations of the whole time period are used for most of the analysis in the study. Six different WRF simulations were conducted that are configured using every combination of the three urban canopy models (SLUCM, BEP, and BEP+BEM) and the two PBL schemes (BouLac and MYJ).

To assess differences between AMDAR observations and simulations, WRF output is trilinearly interpolated in space to the observations to accommodate the flight path. The Mean Bias

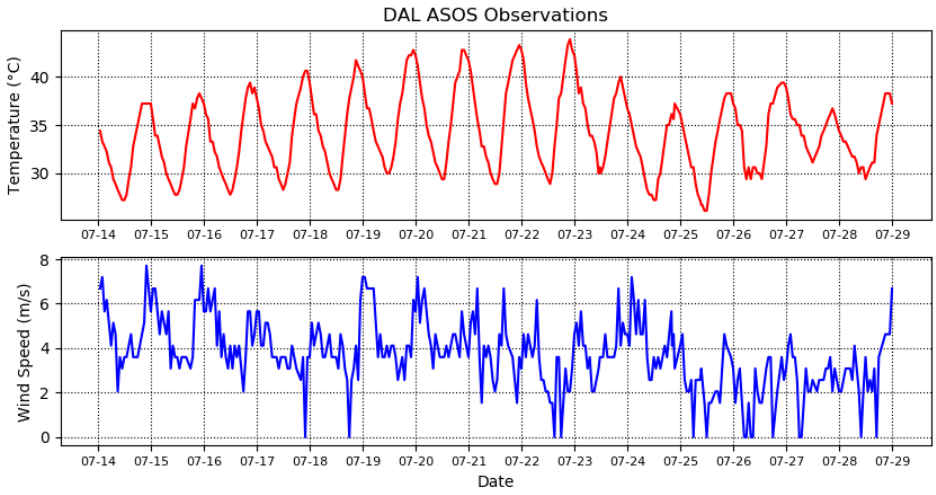

Figure 4: 2m temperature and wind recorded from the DAL ASOS station

Error (MBE) and root mean square error (RMSE) are calculated as

$$\text{MBE} = \frac{1}{N}\sum_{i=1}^{N}(P_i - O_i) \qquad \text{RMSE} = \sqrt{\frac{1}{N-1}\sum_{i=1}^{N}(P_i - O_i)^2}$$

where N is the total number of samples. P represents predicted values (WRF) and O represents observed values (AMDAR). The MBE is a good metric for assessing if there is an average warm or cold bias, but low values can be misleading if there is a high variance in the residuals. RMSE is a good metric for analyzing the degree of error in a simulation, but can be greatly influenced by outliers since it involves the squaring the residuals.

4.1 Surface Observations

Before examining WRF's performance simulating the vertical structure of the atmosphere, it is important to examine the temperature at the surface to provide a more traditional assessment of the UHI. The 2-meter temperature from the WRF and ASOS stations is compared over an urban setting (Dallas-DAL) and a relatively rural setting (Corsicana-CRS) by creating a scatterplot of hourly temperatures (Fig. 5) and the average diurnal cycle (Fig. 6).

For the urban location (DAL), the scatter plots are clustered around the one-to-one line for

the most part. Simulations that use MYJ have a cold bias in the model since more points fall below the one-to-one line. The exception is when the BEM is added to the BEP, which should produce warmer temperatures given that the BEM adds anthropogenic heat sources. The increase of surface temperature from including BEM attests to the sensitivity of the surface energy budget and/or possible positive feedbacks from its inclusion. For both MYJ and BouLac, warmer temperatures exhibit smaller biases than cooler temperatures, with the largest outliers occurring when the observed temperature is coldest.

The average dirunal cycle of temperature reveals small biases during the day and large biases during the overnight and morning hours (Fig. 6). Substantial biases overnight and into the morning occur with simulations using MYJ. The cold bias is mostly offset when BEM is included with BEP. BouLac tends to perform much better over the entire diurnal cycle with less error overnight. The only issue during the day is a collective cold bias when the daytime temperature reaches a peak.

For the rural location (CRS), the scatter plots reveal a ubiquitous warm bias in all simulationsm, the nature of which is undetermined as of yet. Perhaps this can be related to a problem with the boundary condition forcing that the NAM provides. It could also be related to an error in the LSM generation of the surface, leading to poor atmospheric exchange . The MBE for the MYJ simulations is 1.5 °C and for the BouLac simulations is 2.3 °C. Since this is a rural area upwind of the major urban areas, little difference between UCMs is expected. The average diurnal temperature cycle reveals a fairly consistent bias throughout the day with the exception of the MYJ simulations that exhibit a fairly good representation during the early morning hours, which is associated with a stronger surface inversion developing over night, as will be seen in the profiles.

4.2 Profiles

Modeling studies often focus on the importance of parameterizing surface fluxes and surface roughness (Sharma *et al.* 2017) and examining the response of surface temperature. This

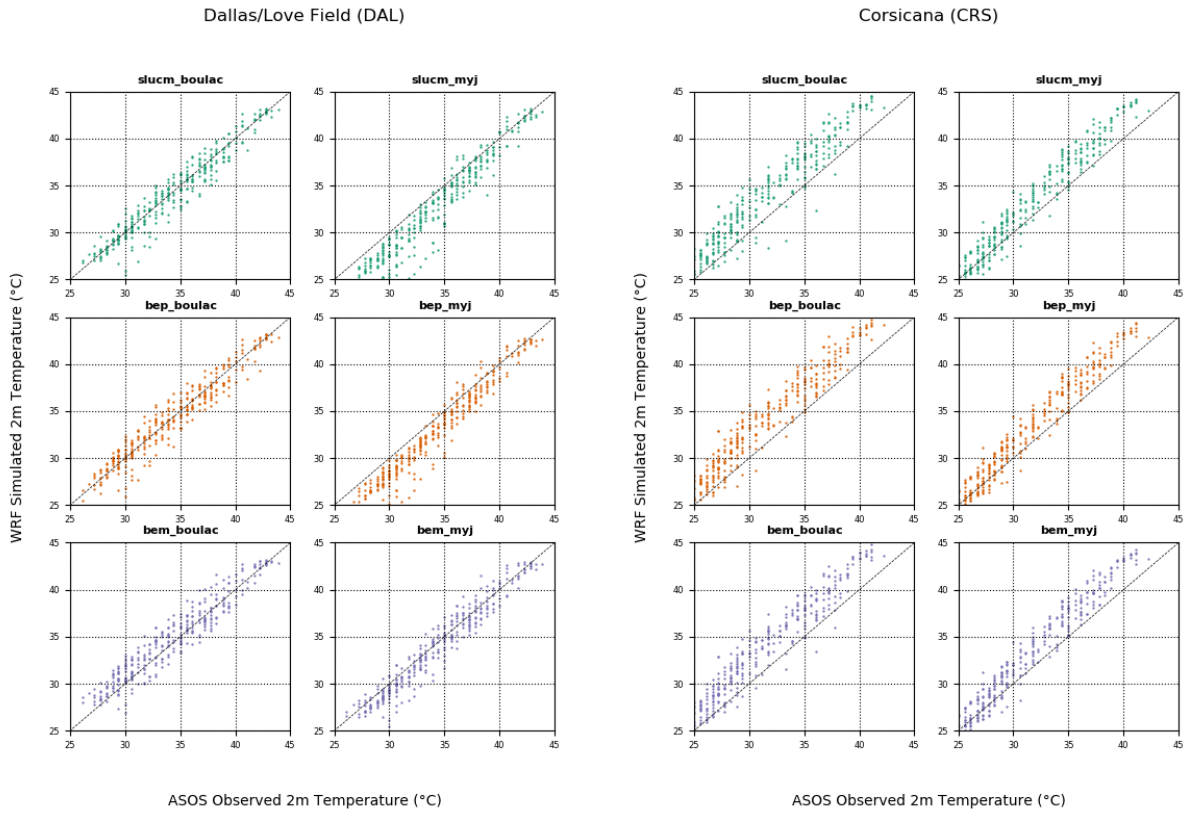

Figure 5: Scatterplots of 2-m temperatures (°C) between the six WRF configurations and the DAL and CRS ASOS stations starting at 0000 UTC 14 July 2018.

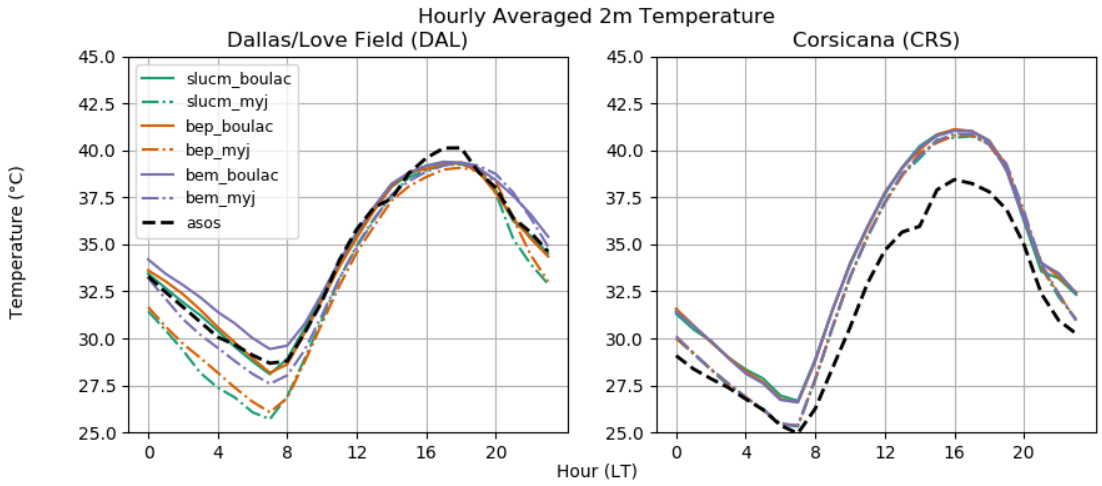

Figure 6: Comparison of 2-m temperatures (°C) between the six WRF configurations and the DAL and INJ ASOS stations starting at 0000 UTC 14 July 2018.

is understandable given that surface observations are readily available and easily used to compare to numerical simulations. Studies that include profiles over urban areas are much more

Table 2: Forecast error metrics 2-m temperatures at DAL CRS

DAL	**MBE**	**RMSE**	**R^2**
slucm_boulac	-0.098	1.16	0.928
slucm_myj	-1.494	2.15	0.923
bep_boulac	0.017	1.19	0.923
bep_myj	-1.313	1.81	0.945
bem_boulac	0.562	1.40	0.908
bem_myj	-0.371	1.21	0.938

CRS	**MBE**	**RMSE**	**R^2**
slucm_boulac	2.316	2.78	0.918
slucm_myj	1.508	2.06	0.956
bep_boulac	2.399	2.78	0.932
bep_myj	1.531	2.05	0.958
bem_boulac	2.338	2.74	0.929
bem_myj	1.582	2.11	0.957

limited, but a number of projects focus on obtaining and examining temperature profiles over urban areas. For instance, the "thermal plume" was originally identified from weather balloon observations over Cincinatti, Ohio (Clarke 1969). More recently, the Urban Boundary Layer Atmosphere Network (UrBAN) in Helsinki, Finland has one of the most comprehensive suite of instruments deployed over a city (Wood *et al.* 2013). The primary measurements of the lower atmosphere over Helsinki come from ceilometers that infer characteristics of the boundary layer from backscatter gradients.

To reduce some of the noise present in individual AMDAR soundings and effectively increase the vertical resolution, all temperature profiles are interpolated to a regular vertical grid with 20-m grid spacing by using all profiles within 30 minutes of each hour from 14-28 July 2018, so these produce a single representative profile for the hour. These hourly-averaged soundings remove some of the noise and minor spatial variability that are seen in the individual profiles and provide a cleaner representation of the vertical profile for that hour.

To highlight differences in the temperature profiles between observations and the suite of simulations, examples of individual profiles are given in Fig. 7, and errors can be grouped into several categories. Although errors occur at all hours, the morning transition is when a the most

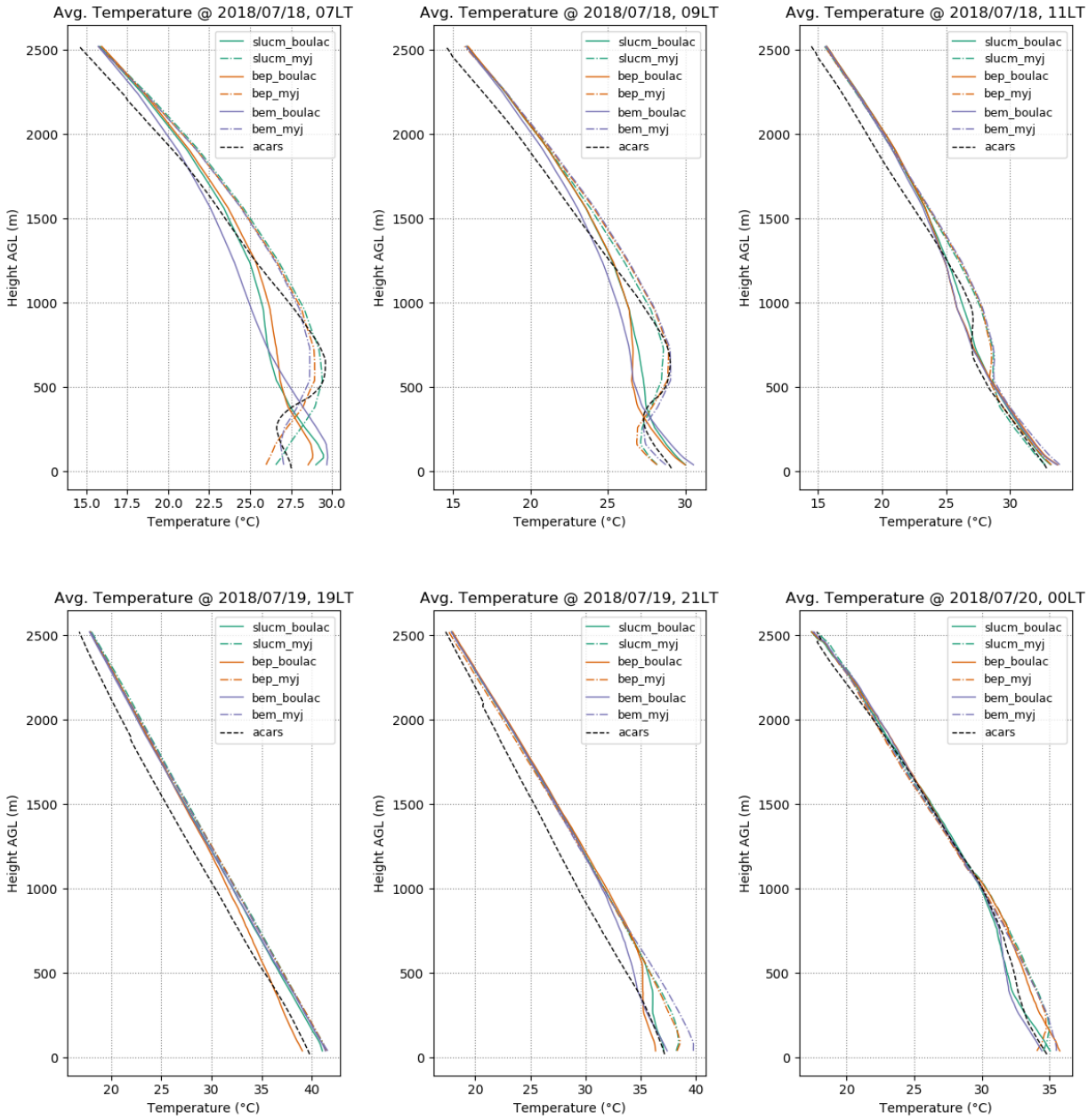

Figure 7: Examples of WRF and AMDAR temperature profiles 14-28 July 2018. Figures a-c show different times representing a morning transition, whereas d-f represent an evening transiton. Specific times are denoted above each profile. WRF configurations are specified in the key.

variation of model errors between configurations is observed.

In the 0800 LT 18 July 2018 profile, the stability of the lower atmosphere exhibits stark contrasts between the model configurations. The simulations using MYJ have a temperature in-

version in the first 300 m while the observations and simulations using BouLac show a profile closer to well-mixed near the surface that is capped by a nearly isothermal layer. The profiles a couple hours later at 0900 LT depict increased mixing near the surface as the PBL deepens with the main differences being the depth of the PBL. MYJ simulations have the shallowest PBL consistent with the more stable lower atmosphere two hours before that inhibits PBL growth. Another two hours later at 1100LT, the PBL has deepened further and the stability aloft weakens. The MYJ configurations generally follow that regime, albeit with the capping stability layer being more isothermal, rather than the slight inversion seen in the AMDAR sounding.

The evening transition, however, shows different characteristics of model performance. An example during the evening transition at 1900 LT 19 July 2018 shows deep, well-mixed profiles. All simulations show a slight warm bias of 1-1.5°C throughout the profile. Most of the differences between the models and the AMDAR soundings begin to occur at 19 LT, and there tends to be a lag between the simulated and observed formation of a nocturnal boundary layer. A few hours later at 2100 LT, more spread in the lowest 500m is shown amongst the simulations as a stable layer begins to form. This layer occurs at different heights, seemingly dependent on primarily the PBL scheme with subtler differences tied to the UCMs. The MYJ scheme tends to show a slight surface inversion, whereas BouLac simulations maintain a lower atmosphere that is closer to well-mixed. The observed nocturnal boundary layer doesn't generally begin to form until around midnight, and the observed temperature profile falls roughly between the MYJ and BouLac in the lowest 750 m.

As an observational baseline, the average hourly lapse rate and the PBL height estimates over the two-week time period from AMDAR are depicted in Fig. 8. In the early morning (05-09 LT), a distinct stable layer is present around 300-500 m with a less stable layer extending down to the surface. The average lapse rate depicts a PBL that becomes better mixed and deepens into the afternoon. A large drop in the average PBL height occurs around 19 LT as the boundary layer becomes decoupled from the surface, leaving a residual layer aloft. The shallow PBL persists throughout the night, but it is noted that there are few soundings overnight compared to other

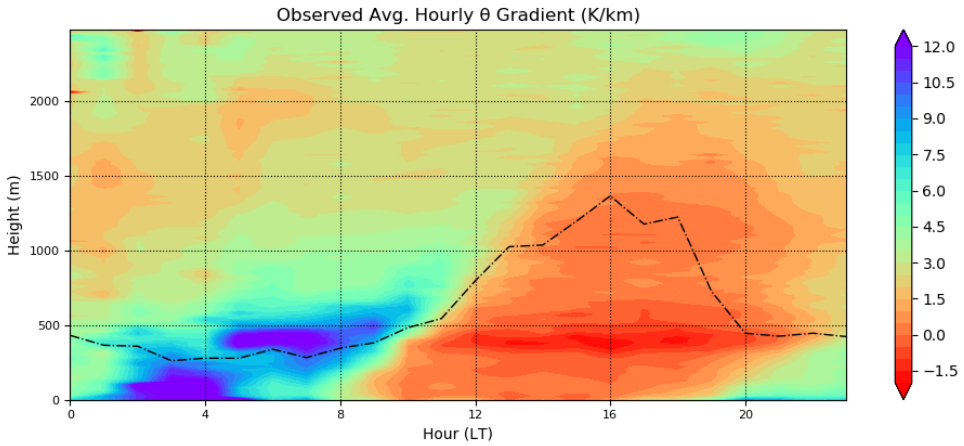

Figure 8: Average dirunal potential temperature lapse rates (K/km) over the period of 14-28 July 2018, with the average Ri_b-derived PBL height overlayed as a black line

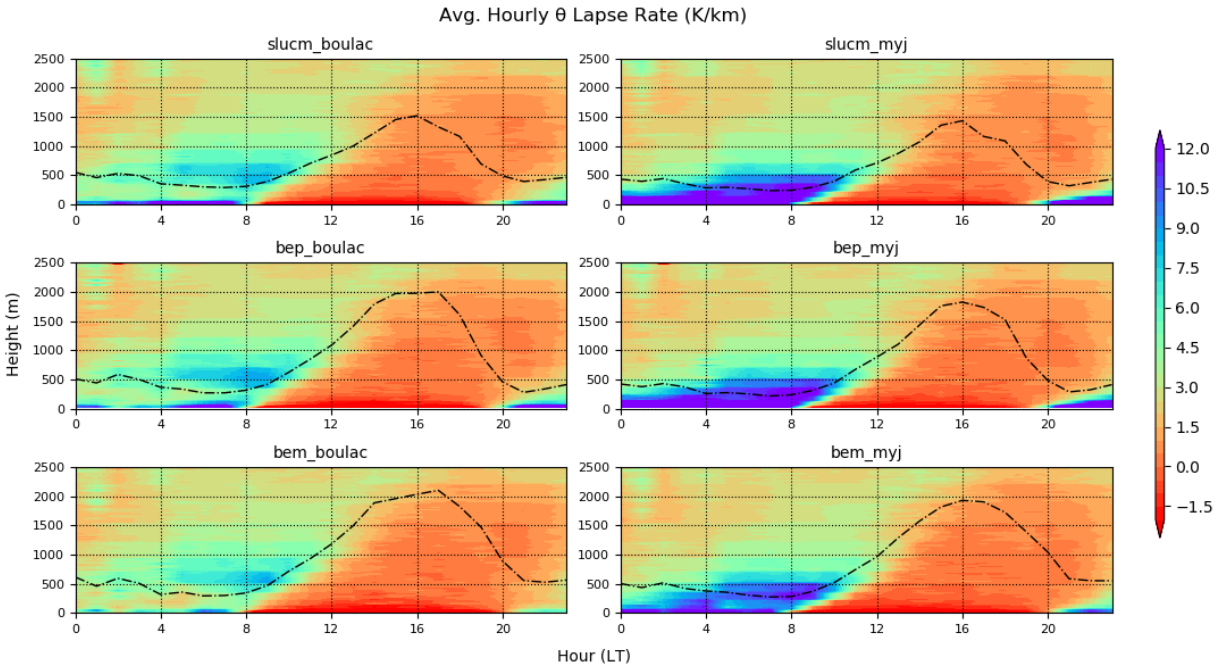

Figure 9: As Fig. 8, but for WRF-simulations indicated above each panel

parts of the day that have more air traffic. From midnight to 4LT, there are as few as 8 soundings at a particular hour for the entire two-week period. Observations improve at 05 LT when there are 38 soundings over the two week period, and the number jumps up to 374 soundings at 06 LT and even more during the day and evening.

As expected, the general diurnal cycle is seen in all of the WRF simulations (Fig. 9). Each

WRF configuration simulates the general features of the PBL height and the lapse rate, but as already seen in examples from individual soundings, there are nontrivial disagreements with the heights at which the inversions occur and the magnitude of the lapse rates, especially overnight and during the morning hours. The most striking difference is between the two PBL schemes with much stronger lapse rates associated with MYJ and much weaker lapse rates with BouLac. Subtler differences between the UCMs are also present, but much less obvious.

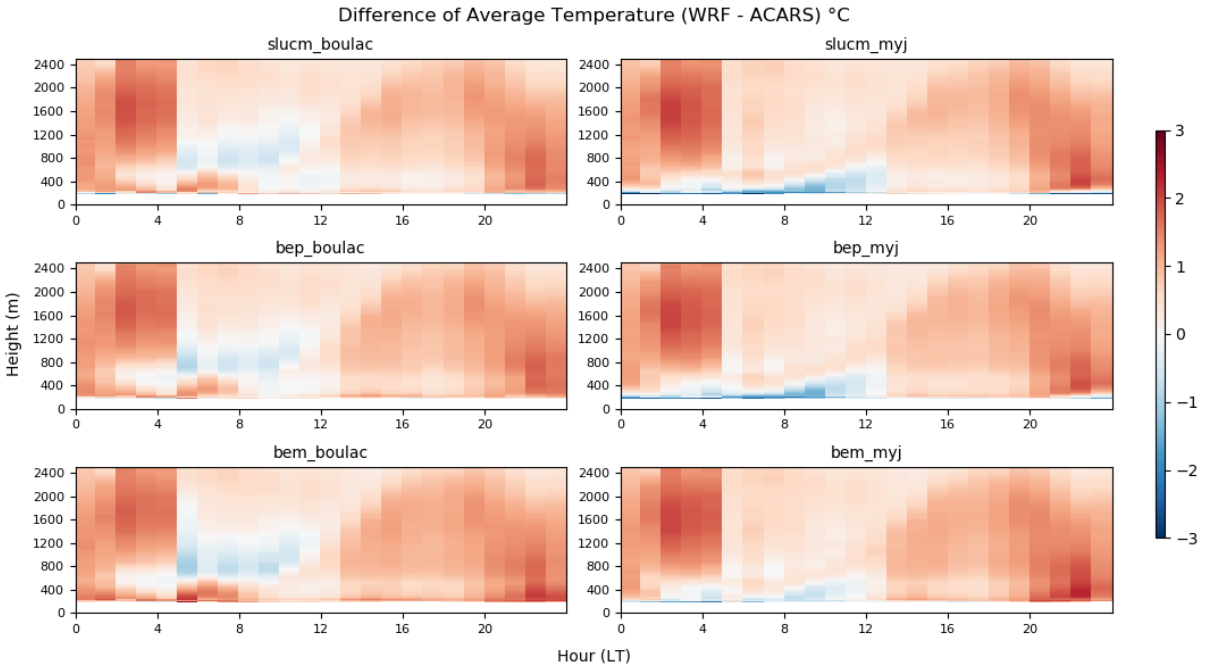

Figure 10: Temperature (°C) differences (WRF-AMDAR) in the diurnal cycle

Using AMDAR observations as the baseline, the diurnal cycle of temperature for each simulation is compared to the diurnal cycle obtained from the observations (Fig. 10). During the day all configurations exhibit a warm bias within the PBL with smaller differences aloft. There appears to be a large warm bias overnight, but the paucity of observations during this time period (00-05LT) prevents any sweeping conclusions from being drawn. During the 07-12LT period when there is ample data, a vertical dipole of errors is evident. Simulations using BouLac have a warm bias near the surface and a cool bias aloft, indicating that the lower atmosphere over the city is less stable than observed. Simulations using MYJ have a cold bias near the surface and a warm bias aloft, indicating that the lower atmosphere is more stable than observed. These

dipoles are consistent even with different UCMs, although the model output using BEP+BEM dampens the errors produced by MYJ and the lapse rates approach values closest to the AMDAR observations.

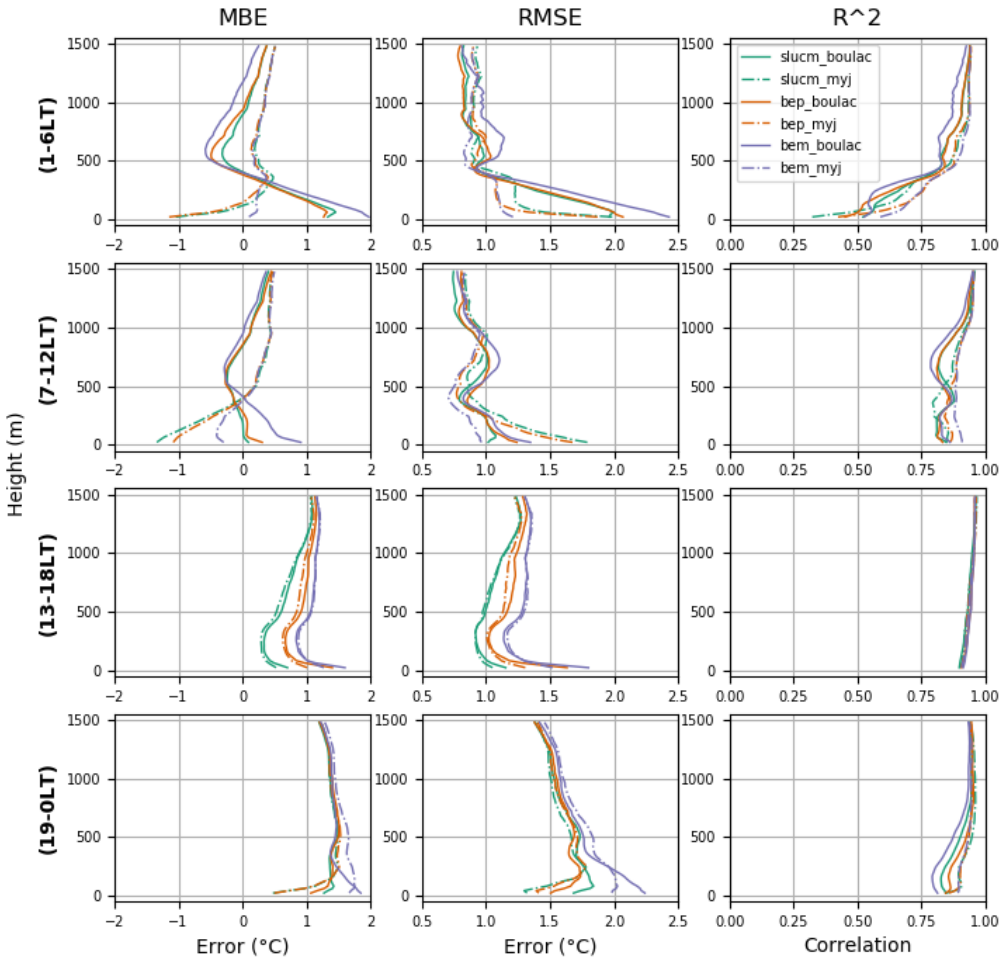

Figure 11: Forecast error metrics for (a) overnight, (b) morning, (c) afternoon, and (d) evening. All metrics are displayed vertically for each height level AGL.

To quantify the differences between simulations and AMDAR, the day is divided into four periods (Fig. 11), defined as overnight (01-06LT), morning(07-12LT), afternoon (13-18LT), and evening (19-00LT). Largest errors occur overnight, in part due to less frequent observations that impact these metrics. Errors are greatest near the surface with biases 1-2 °C and RMSE decreas-

ing from 2 °C near the surface to 1 °C at 500 m. A dipole in the bias exists with BouLac exhibiting a warm bias at the surface and cool bias aloft between 500-1000 m, while MYJ has a cool bias at the surface and warm bias aloft. Correlations overnight are low near the surface, but improve aloft.

During the morning hours, the same general biases are found, but simulations using BouLac generally perform well below 400 m. MYJ suffers from a 1 °C cold bias at the surface changing sign around 400 m to a warm bias. For both MYJ and BouLac, the simulations with BEP+BEM tend to be warmer at the surface but approach the profiles of the other UCMs above 400 m. In the afternoon, all configurations perform similarly with a warm bias ranging from 0.5 °C at the surface for SLUCM to 1 °C for BEP+BEM. It is noteworthy that there is little difference between MYJ and BouLac during the day and that the differences are attributed to mainly the UCMs.

The modeled θ lapse rates seen in Fig. 9 and average soundings seen in Fig. 11 provide more evidence that the BouLac PBL scheme allows for simulation of a better mixed lower atmosphere and a thicker UBL than the MYJ in the morning. The MYJ scheme tends to stabilize and cap the mixed atmosphere immediately above the urban surface. However, the heat anomalies represented in urban surface through the UCM are indeed contributing factor. The BEP+BEM scheme in particular simulates a hotter (and generally less erroneous, as per Fig. 6) urban surface, which seems to have implications in the vertical profile as it promotes a less stable environment. When the BEP is coupled with the BEM, the temperature profiles approach what is seen in the observations during the morning, which is also consistent with the low error seen in the BEP+BEM and MYJ configuration.

Examining the evening transition shows a slightly different behavior between model configurations. The MYJ simulations tend to have a positive lapse rate bias near the surface. Even the BEP+BEM and MYJ configuration caps the evening transition moreso than in the observations. The BouLac configurations also show a relatively stable layer developing during the evening hours, but when coupled with the BEP+BEM UCM, the near-surface environment is not as stable and the θ lapse rates are not as strong, which is more consistent with the observations.

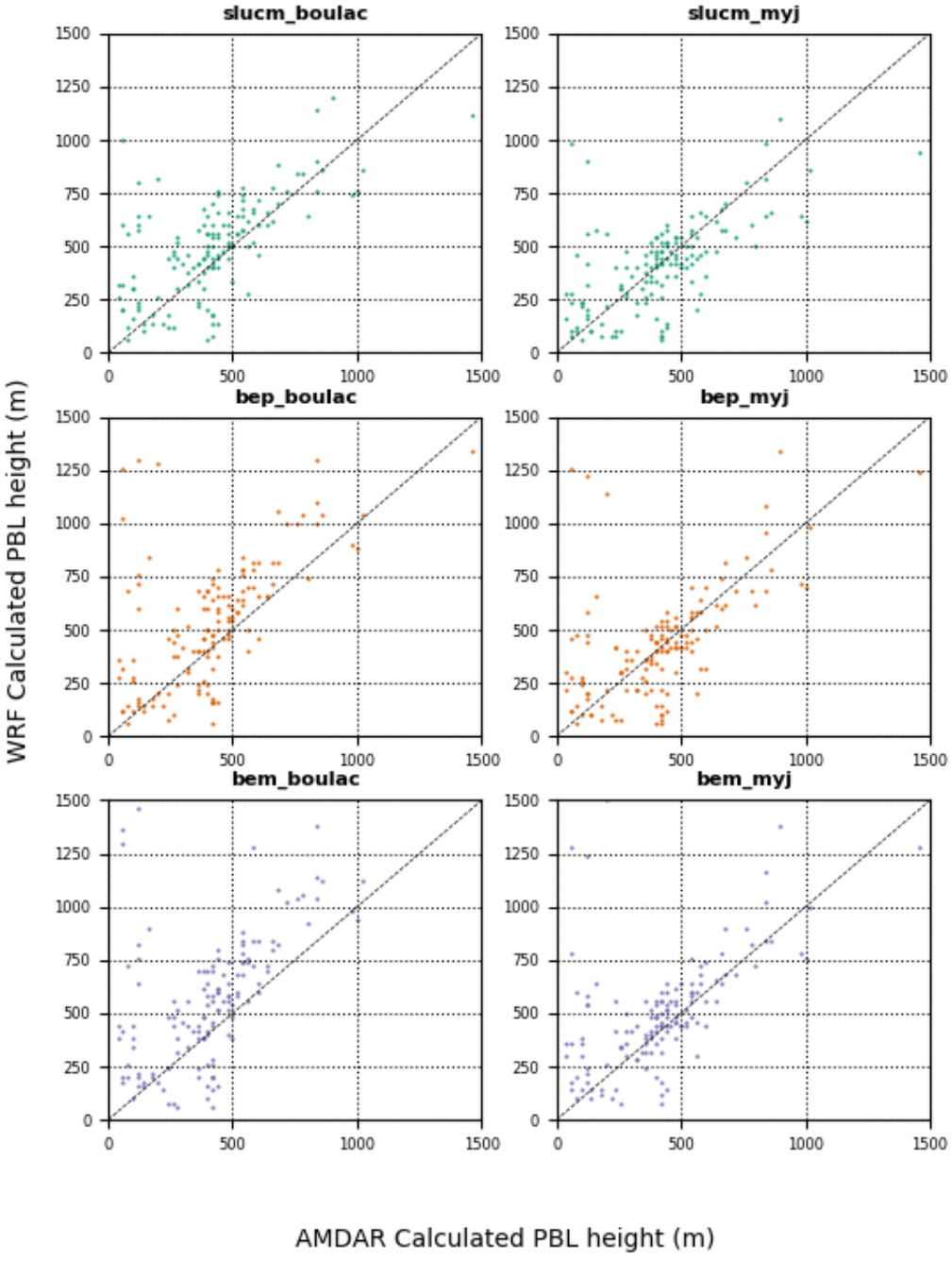

Figure 12: Scatterplots of Ri_b-derived PBL heights (m) between the six WRF configurations and the DAL and DFW AMDAR soundings starting at 0000 UTC 14 July 2018.

Table 3: Caption

Configuration	MBE	RMSE	R^2
slucm_boulac	76.7	219.1	0.458
slucm_myj	-9.6	200.0	0.458
bep_boulac	125.5	283.5	0.397
bep_myj	13.8	232.0	0.389
bem_boulac	164.6	330.7	0.348
bem_myj	79.4	251.3	0.370

The Ri_b-derived PBL heights from the six model configurations are compared to heights found from AMDAR (Fig. 12). While there is a fair amount of scatter between the PBL height estimates, there are some general features seen among the configurations. The R^2 values are between 0.37-0.46 with RMSE from 200-330 m (Table 3). Many of the heights fall near the one-to-one line, but large overestimates of PBL heights by the model occur when the AMDAR-derived PBL height is low. MYJ produces PBL depths at similar levels closer to the AMDAR estimated values, or heights that are more symmetric about the one-to-one line in Fig. 12. This dichotomy is reasonably consistent with the θ gradients seen in Fig. 9, which indicated the BouLac schemes tended to have less stable conditions near the surface than the MYJ schemes.

4.3 WRF Downwind Analysis

Previous sections examine the lower atmosphere near the center of the Dallas-Fort Worth UHI, but there could be significant non-local impacts extending downwind of the city to rural areas, which may be heavily influenced by the particular suite of parameterizations. Downwind impacts are related to the "urban plume" (Cosgrove & Berkelhammer 2018) and depends on the direction of the wind, so a series of along-flow cross sections are created to highlight downwind and upwind impacts of each model configuration (Fig. 13). DAL is used as the center for these plots, and the average 10-m wind over the entire domain is used to create hourly cross sections 100 km upwind and 100 km downwind of DAL. The edge of the most dense urban areas is roughly 30 km away from DAL. These hourly cross sections orientated to the wind direction are used to create averages for the different time periods over the day. Because this is a summer

heatwave case, the wind is primarily southerly across the whole domain and the day-to-day variability is relatively small.

4.3.1 Lapse Rates

The lower atmosphere over urban areas is generally warmer and less stable than the surrounding rural areas overnight and into the morning (Godowitch *et al.* 1985; Baklanov 2002). As a result, the prevailing wind can transport the warmer air from the urban center downwind and over a cooler layer near the surface over rural areas. This phenomena has been observed and modeled, and it is referred to as the "urban plume" that can extend 70 km downwind of the urban center (Cosgrove & Berkelhammer 2018). When examining the simulated temperature profiles above the city, it is also important to understand biases upwind of the city that are driven by mainly the PBL schemes since no substantial urban areas are present so the UCM does not play a role in the upstream rural areas. To investigate the sensitivity of the downwind and upwind impacts to the model configuration, potential temperature (θ) lapse rates and temperature lapse rates are evaluated. Negative distances are upwind of DAL and positive distances are downwind of DAL.

As seen in the soundings over the urban areas, the smallest differences between configurations occur during the day when the atmosphere is generally well-mixed over a deep layer, so this section focuses just on the substantial differences that occur overnight into the early morning hours (01-06 LT). This time also corresponds to the most stable part of the day that can most effectively trap pollution near the surface, which has direct impacts on public health.

According to Fig. 13, the three WRF configurations that produce a more mixed UBL during the overnight to early morning hours are the ones that utilize the BouLac PBL scheme. One notable exception is the combination of the BEP+BEM UCM and the MYJ PBL scheme, which shows a small area that is less stable than its surroundings that stretches from the DAL urban center to 30-40 km downwind before encountering the more stable atmosphere over the rural areas.

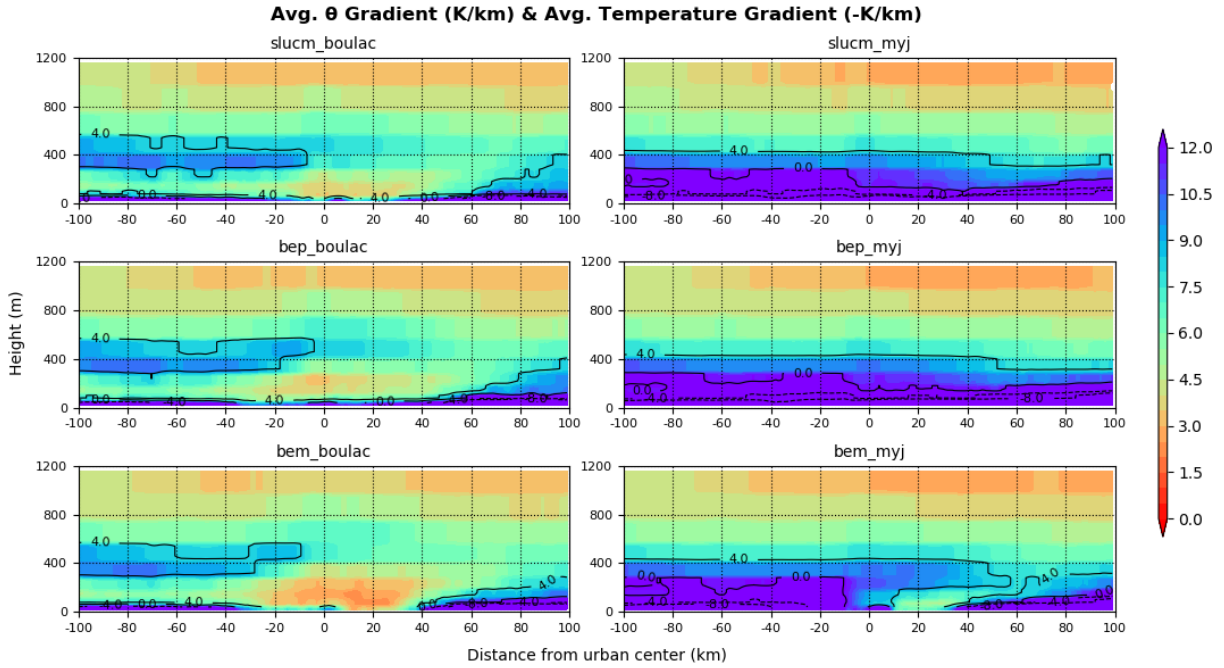

Figure 13: Average along-wind cross-sectional potential temperature lapse rates during the overnight/morning hours (01-06 LT) from 14 July to 28 July 2018

Although the temperature structure over the city is the most pertinent to public health, it is obvious that the upwind temperature profiles are vastly different between the two PBL schemes. BouLac exhibits a very shallow stable layer near the surface, with a weakly stratified layer that is capped by a more stable layer around 400 m. On the other hand, MYJ has a stable layer extending up to about 400 m. As this layer is advected over the city, the shallow layer in BouLac can be mixed out more easily than the deep stable layer present upwind of the city produced by the MYJ scheme.

Simulations incorporating the BouLac PBL scheme produce noticeable urban plumes downwind. The temperature structure does not mirror the upwind structure, resulting in an asymmetric cross section. Warmer temperatures advected downwind and over the top of the shallow surface layer developing over the rural areas can act to stabilize the lower atmosphere, resulting in greater lapse rates that extend deeper than those seen upstream. Since the MYJ scheme promotes a deeper stable layer near the surface than BouLac, mixing of the more stable layer as it advects over the city would be more difficult, with the exception of the stronger impacts of

BEP+BEM, indicating that the UCM does indeed influence downwind effects.

This sensitivity study suggests the selection of PBL scheme dominates the model output when compared to the differences driven by the various UCMs. The UCM selection does influence the near-surface temperature anomalies and at some level there are more nuanced interactions between the UCM and PBL, but the PBL is by far the greatest factor. Fig. 13 demonstrates that the BouLac closure scheme promotes an environment conducive to better-mixed profiles over the urban area.

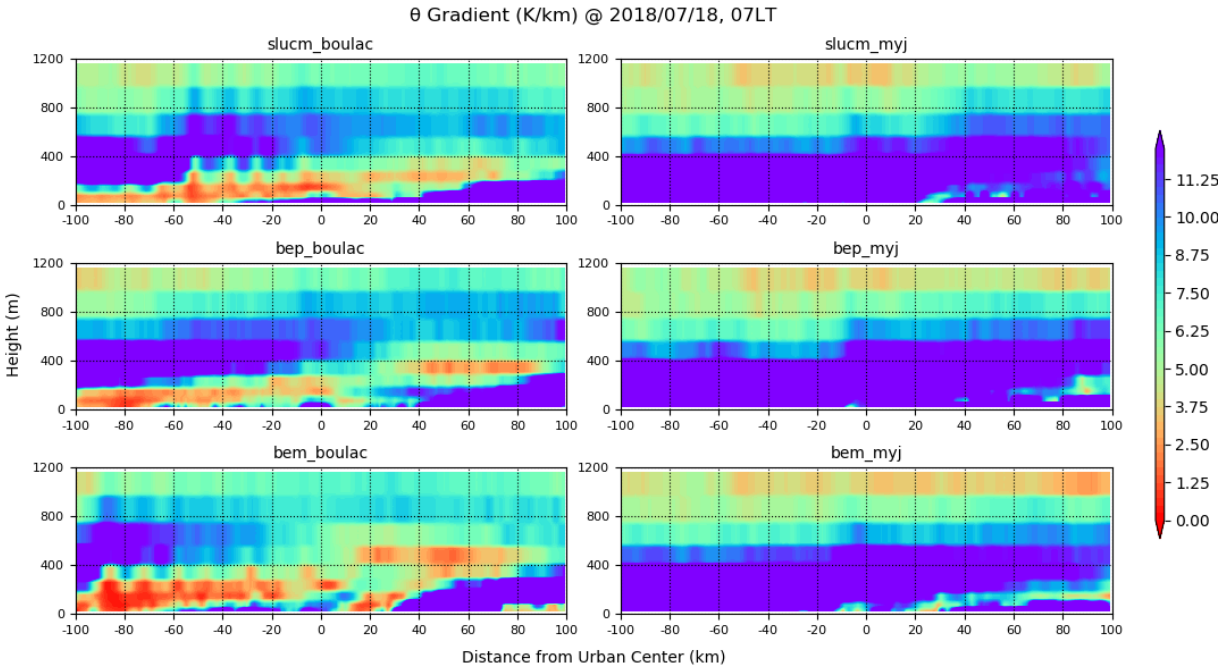

Figure 14: As Fig. 13, but for 07 LT 18 July 2018.

While focusing on the mean data provides a generalized look at the differences, it is instructive to make a case-by-case comparison with the soundings in the previous section (Fig. 7). Matching each case with AMDAR soundings from the same hour helps visualize the departures of the simulated temperature profiles from the profiles obtained from AMDAR. The focus starts with a series of along-wind plots surrounding the morning transition phase of 18 July 2018 (top panels of Fig. 7), and end with the evening transition case during 19-20 July 2018 (bottom panels of Fig. 7).

Beginning at 07LT 18 July (Fig. 14), corresponding to the time of the first sounding in Fig. 7,

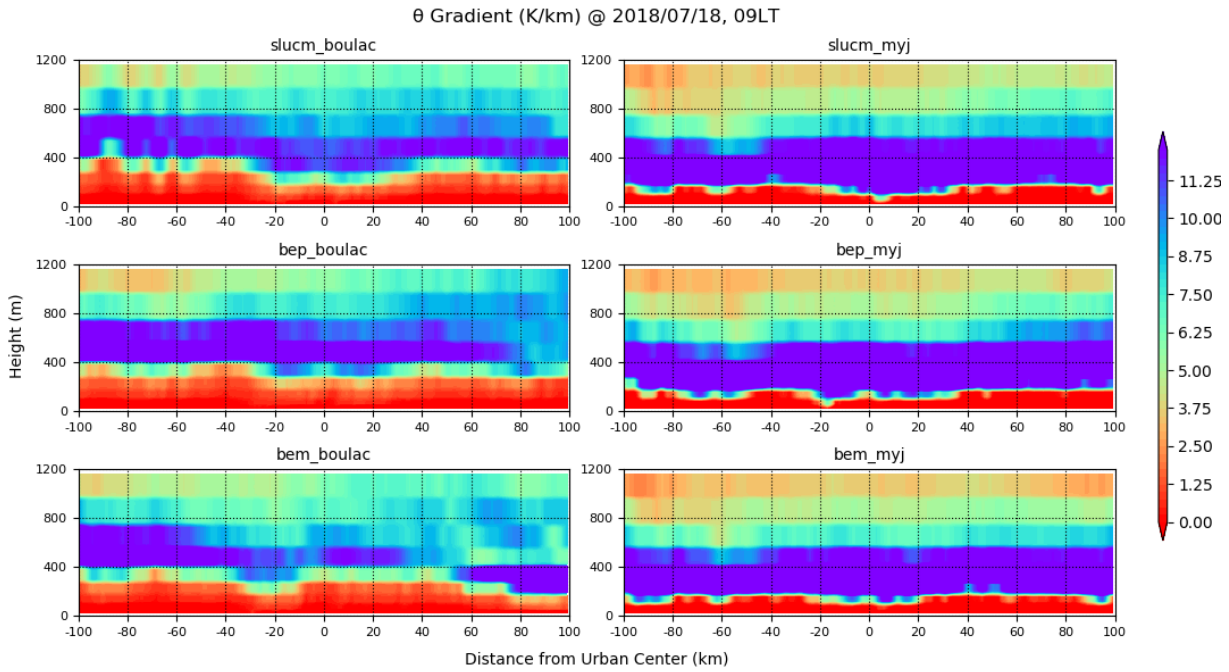

Figure 15: As Fig. 13, but for 09 LT 18 July 2018.

the stability upwind of DAL is much different for the MYJ and BouLac schemes. For simulations using BouLac, there is a shallow layer near the surface with low stability, that is underneath a stable layer centered around 400 m. As the shallow, low stability layer is advected over the city, it generally deepens and the stable layer is eroded. This plume extends downwind above a stable layer that forms near the surface just downwind of the city. The stable layer deepens further downwind while the low lapse rates associated with the plume from the city dissipate. All three UCMs used with BouLac behave similarly, but the magnitude, depth, and extent of the features seen in the lapse rates differ slightly with the BEP+BEM configuration exhibiting the greatest depth and lowest stability over the center of the city, which can also be seen in the individual soundings (Fig. 7).

For simulations that use MYJ, there is a deep stable layer upwind of the city with very little change seen directly over DAL. There is some evidence of a lapse rate change in a small layer just downwind of the city center, but it is a marginal change. With such a stable layer upwind of the city, it is not surprising that any surface forcing is suppressed since it has to overcome the strong stability advected over the city.

Two hours later, shortly after sunrise (Fig. 15), all configurations depict a well-mixed layer at the surface over the entire cross section. The most noticeable difference is again between the PBL schemes. BouLac has a deeper layer that extends from the surface up to about 400 m where a stable layer begins. Given the much more stable conditions overnight in MYJ, it is not surprising that two hours later the mixed layer near the surface is much shallower than BouLac, and a very stable layer remains just above, starting at about 250 m. In the BouLac and BEP+BEM configuration, Only a faint signal remains of the urban plume that was once easily seen in all of the 07LT BouLac cross sections.

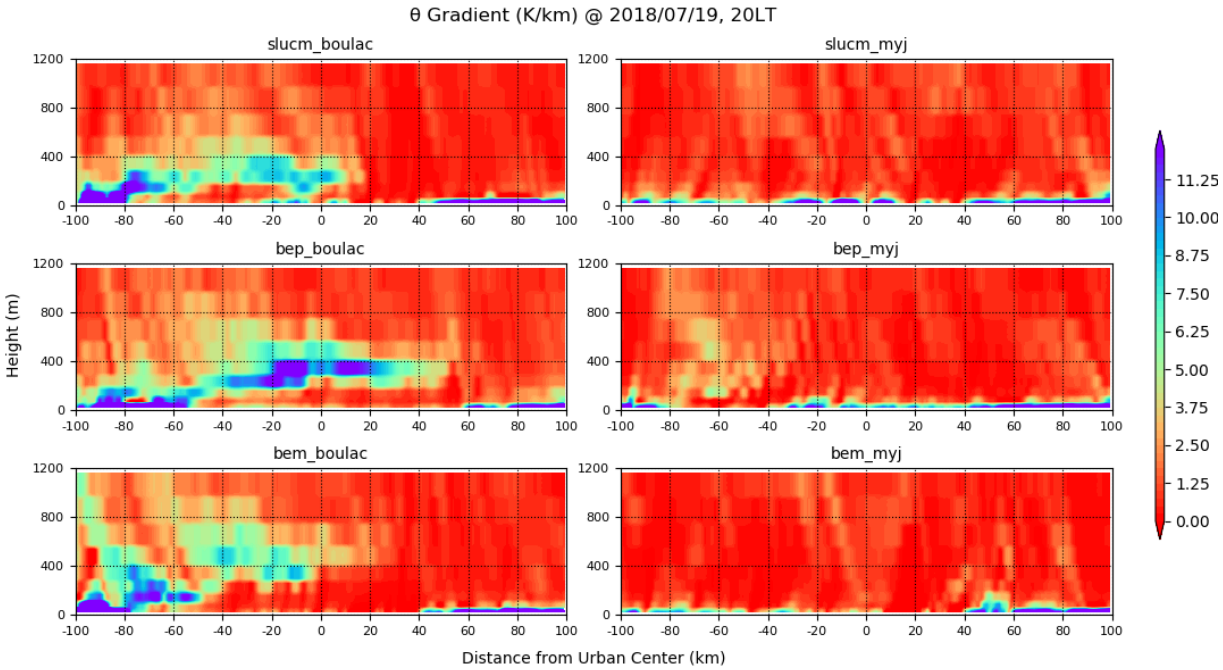

Figure 16: As Fig. 13, but for 20 LT 19 July 2018.

Another series is analyzed showing the evening transition case during 19-20 July 2018. Figs. 16 - 18 show an early emergence of a rural stable layer forming upwind of the urban area in the BouLac configurations at 20 LT, whereas the MYJ is still in a largely mixed regime aside from the near-surface stability. The BEP+BEM is the only UCM that shows a near-surface heat anomaly over the urban center that is surrounded by shallow stable layers both up and downwind ranging from 40-100 m AGL.

For the configurations using BouLac, two hours later at 22 LT the stable layer lifts from the

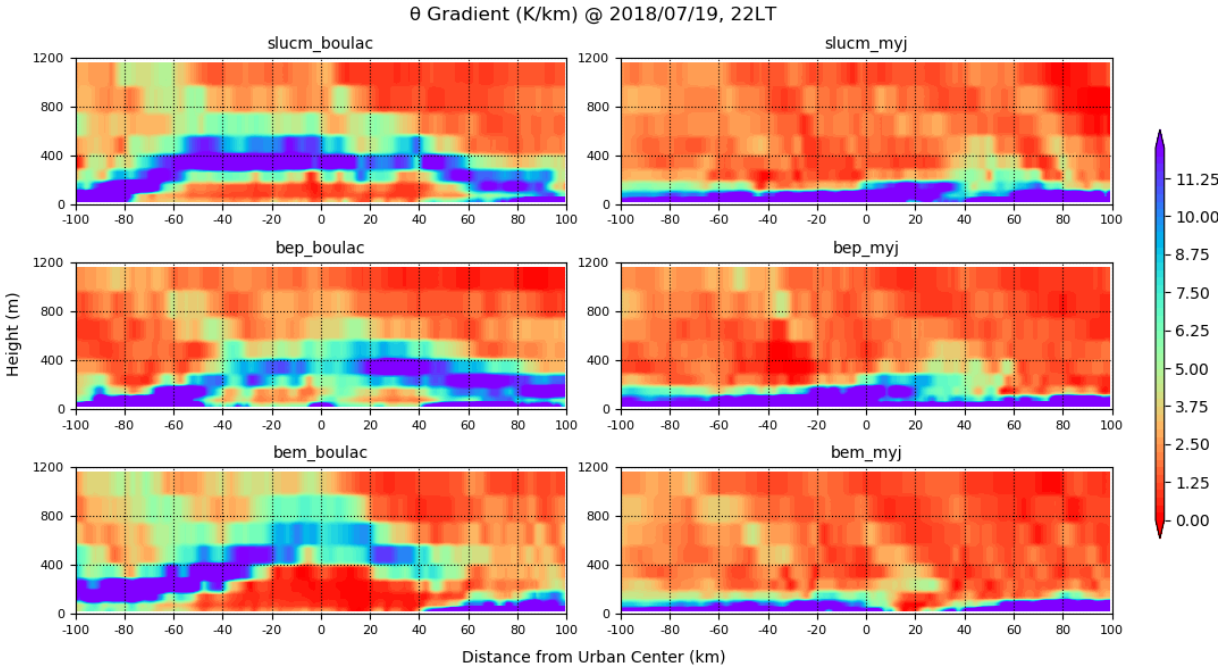

Figure 17: As Fig. 13, but for 22 LT 19 July 2018.

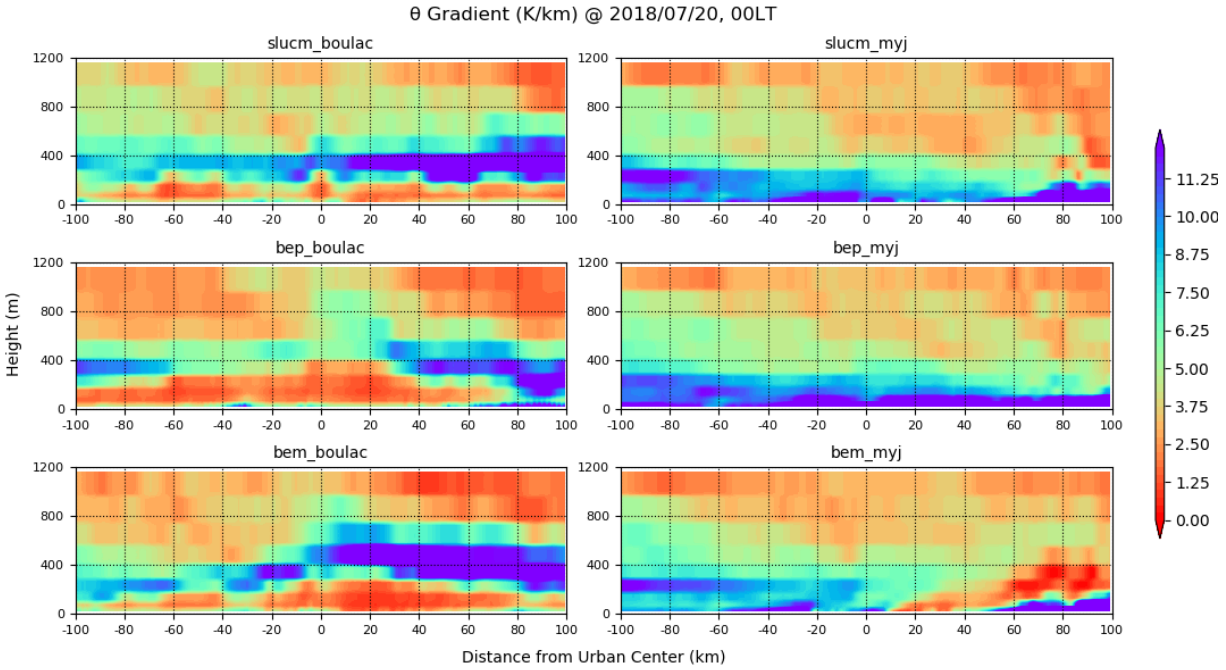

Figure 18: As Fig. 13, but for 00 LT 20 July 2018.

near the surface upwind of the city over a well-mixed layer over the urban center and then back towards the surface resulting in a "bulge" over the city. This bulge is particularly enhanced

when BouLac is coupled with BEP+BEM. In contrast, simulations that use MYJ shows a stable layer developing at the surface over almost all the domain excpet twoards the downwind edge of the urban center with a slightly shallower surface stable layer downwind of the urban center.

By midnight, there are some downwind effects visible with the BouLac scheme, but the mixed layer near the surface has not quite penetrated the stable layer. The MYJ scheme, conversely, shows a mostly even stable layer near the surface. The BEP+BEM coupling counters the other MYJ configurations by showing a prominent downwind plume extending from the urban center and reaching to at least 100km. This demonstrates that the urban plume in the BEP+BEM and MYJ configuration can exist in the early part of the night with practically no single in the MYJ simulations that use just BEP or SLUCM.

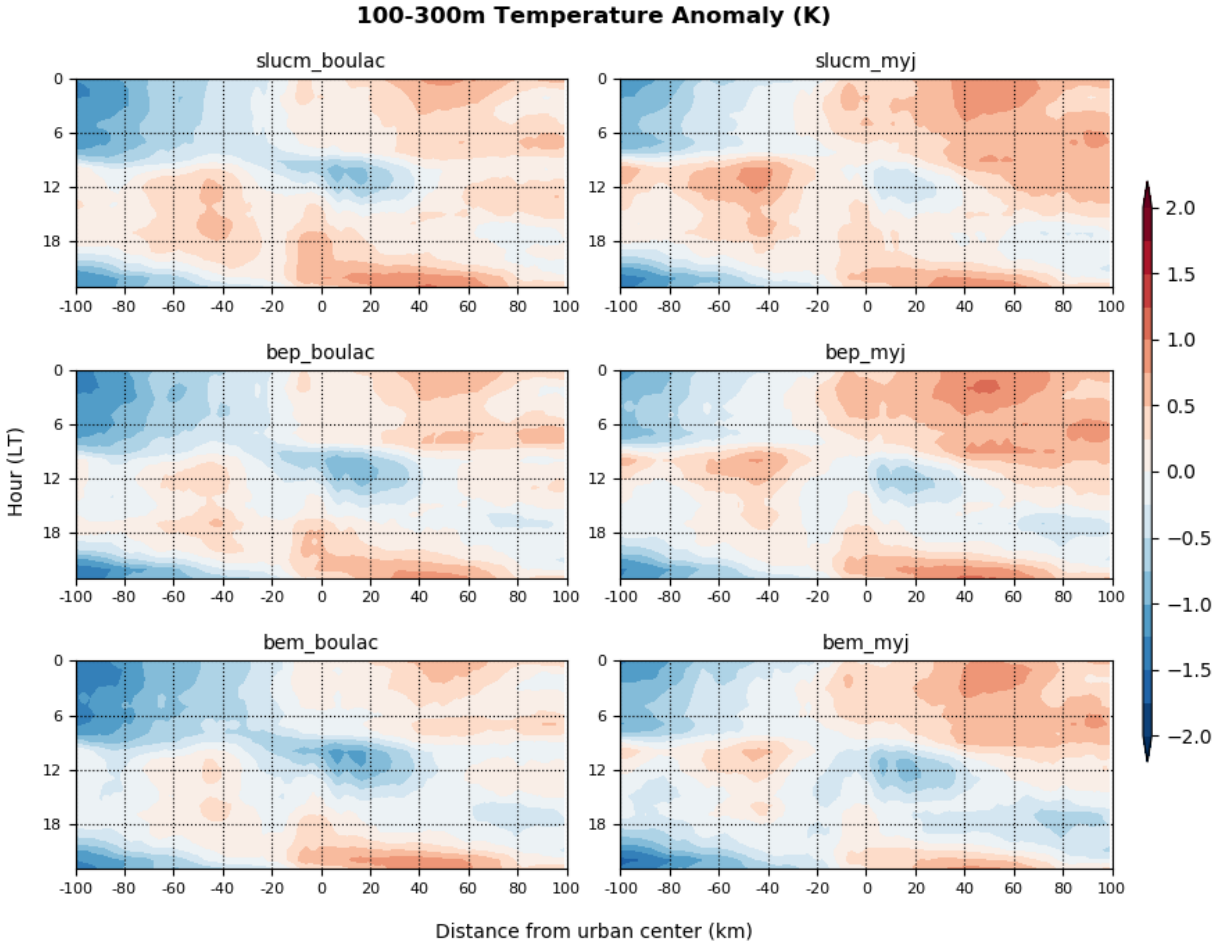

Figure 19: Average wind-direction cross-sectional temperature anomalies averages over the diurnal cycle from 14 July to 28 July 2018.

Another signature of an urban plume can be found in the 100-300 m downwind temperature anomalies, as seen in Fig. 19. Each configuration shows that there is a clear downwind positive temperature anomaly downwind of the urban center from about 20 LT to 12 LT the following day. However, the strength of this anomaly is vastly different based on the choice of the PBL scheme. BouLac simulations tend to dampen this anomaly compared to MYJ simulations. This can be attributed to the generally well-mixed environment upwind as well as downwind of the urban center in Fig. 13. Another interesting feature in this figure is the wavelike progression of the negative temperature anomaly that is present to some extent in all the simulations. At around midnight, there is a strong negative temperature anomaly upwind of the urban center, before it progresses towards the urban center at noon, and then further downind going into sunset. However, the warm anomaly originating at the urban center dominates downwind after sunset and continues into the night and the following morning.

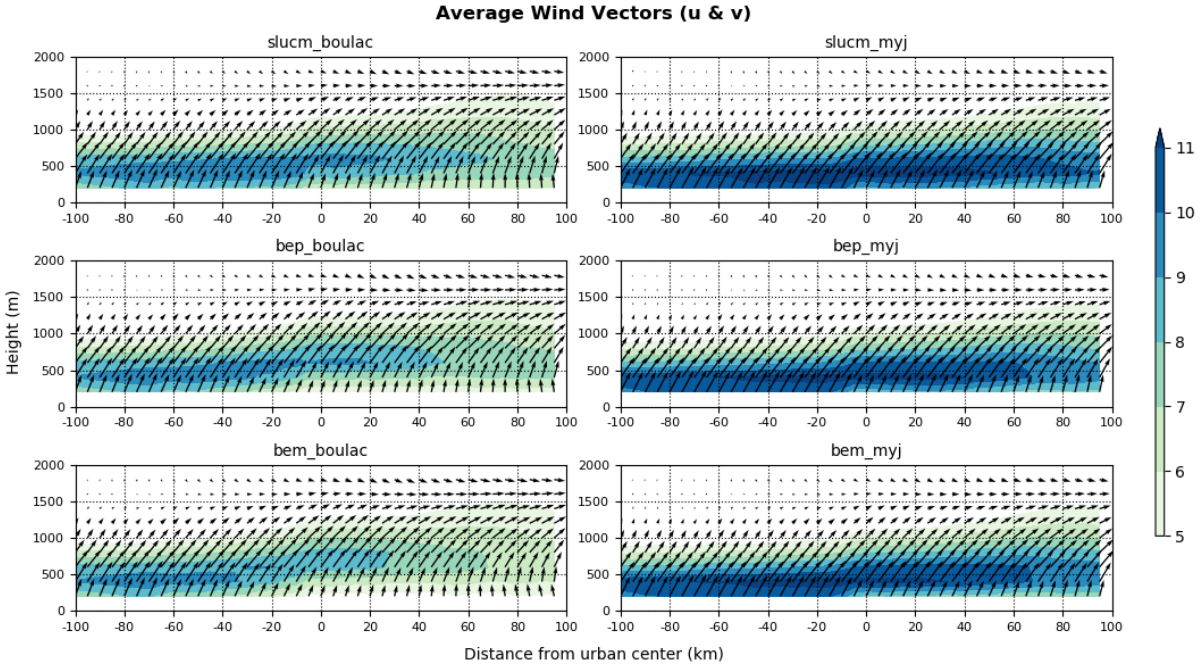

Figure 20: Average wind-direction cross-sectional potential temperature lapse rates during the overnight/morning hours (01-08LT) from 14 July to 28 July 2018. Wind directions are indicated by the vectors, with wind magnitude contoured in the background.

Fig. 20 takes a turn away from the lapse rates and focuses on the amount of wind shear

present in the simulated atmosphere. Within the Bulk Richardson number, turbulence is focused in on two components: thermally-generated shear and mechanically-generated shear. What this cross-section shows is that during the morning hours, the winds generally blow from the south and show some veering towards a smaller easterly flow aloft. Overall, there isn't much of a disparity in simulated windflow direction in the model configurations. The MYJ simulations exhibit a large amount of magnitude shear, however, which is associated with the stable regime demonstrated by the downwind θ lapse rates.

5 Discussion & Conclusions

Two main impacts that motivate this work are: (1) surface temperature is important for heat-related illnesses (e.g., Frumkin 2002; Murage *et al.* 2017) and (2) the temperature profile in the lower atmosphere determines the stability and therefore the dispersion of pollution emitted at the surface. Since numerical weather prediction is an integral component for forecasting and warning heat waves and high-impact pollution events, the model's ability to simulate the atmospehre over a city is examined. The two main impacts are related and are both primarily influenced by the UCM and PBL scheme, and it is demonstrated here that the model output can vary greatly between simulations as the examples in Fig. 7 illustrate.

Given that most studies focus on the surface temperature since those observations are the most readily available for model verification, the simulated temperature profile in the lower atmosphere is not discussed as often as the simulated surface temperature. Observations from commercial aircraft over major cities now provide an ample source of measurements and allow more detailed examination of how numerical simulations handle the lower atmosphere over an urban area. Aircraft observations from AMDAR provide the benchmark for model output over the city, but the relative differences between each configuration are also explored in more depth. Further away from the airports over the rural areas, the observations near the airports are too far away to provide a direct comparison, so the model intercomparison is the only way

to assess features such as the urban plume but reveal important differences in what happens directly over the city.

The Dallas-Fort Worth area was selected as the test site because the topography is relatively flat, there are no coastal influences that could dominate the diurnal cycle, and there are ample AMDAR observations available. The period of 14-28 July 2018 was selected since it was a long period of relatively hot but otherwise quiescent weather conditions as shown by Fig. 4.

Simulations were conducted using WRF and used two domains with the inner nest having a grid spacing of 1 km. The initial coniditons and lateral boundary conditions come from NAM and information on the built environment are obtained from NUDAPT. Given the sprawling urban area of Dallas-Fort Worth, it is expected that the two most important model parameterizations are the UCM and the PBL schemes. The two PBL schemes (BouLac and MYJ) that are coupled with the three UCMs (SLUCM, BEM, and BEP+BEM) were used to simulate the Dallas-Fort Worth region over the two week period, resulting in 6 different configurations.

Beginning with the surface temperature, which is the most commonly used metric to test model performance, all six of the configurations contained a similar warm bias of the 2-m temperature over the rural station. For the 2-m temperature at DAL, larger differences were apparent with a notable difference in the overnight and morning temperatures. Simulations using MYJ with SLUCM and BEM had the largest cold biases, but when the BEP+BEM was used, the bias was much less. All simulations using BouLac for the surface temperature performed much better simulating the 2-m temperature at DAL.

Temperature profiles above DAL reveal a range of model solutions that have vastly different implications for surface temperature and stability in the lower atmosphere, both of which are important for understanding health impacts from heat stress to the concentration of near-surface air pollution. During the day when the PBL is deep and well-mixed, little difference between the six configurations can be seen. The greatest differences occur over night and into the early morning, which correspond to the largest difference in the 2-m surface temperature.

All simulations with MYJ produce a much deeper stable layer near the surface than simula-

tions with BouLac. At most a very shallow temperature inversion occurs with BouLac, but the atmosphere under 500 m is generally much less stable than what MYJ produces. The strong inversion layer in MYJ is related to the large cold bias noted in the 2-m temperature and also has implications related to air pollution since vertical mixing is suppressed and the stability lasts longer into the daytime. As a result, model output using MYJ would underestimate the intensity of the urban heat island in the morning and overestimate the air pollution. It is important to note that a cooler temperature overnight has been identified as a critical factor in reducing heat-related illnesses and morbidity in urban areas (e.g. Murage *et al.* 2017; Frumkin 2002).

The diurnal cycle of each model configuration was compared to the dirunal cycle obtained from AMDAR (Fig. 10). The daytime boundary layer is generally warmer than observed in all simulations. The most prominent errors are seen during the morning hours and appear as vertical dipoles of model bias, again indicating weaker stability in the BouLac simulations and stronger stability when MYJ is used. Influence of the UCM can be seen in this figure and the strong stability of MYJ is reduced when BEP+BEM is used. This is attributed to the increased anthropogenic heating when BEM is included, so the biases in this configuration are smallest on average. However, it is noted that the impact of the PBL scheme is by far the dominant factor.

Although AMDAR observations of the lower atmosphere occur near the center of the UHI, non-local impacts are another important component to consider since errors upstream of the urban area can propagate into the area and then interact with the UCM over the city, which will effect the urban area and also extend downwind. Mean cross sections in the along-wind direction were constructed to reveal how the atmosphere was modified as it moved over the city and then advected further downwind. Largest differences again occur during around early morning hours. Given the weaker upwind stability in BouLac overnight and into the early morning, a deeper mixed layer forms over the city with a clear plume extending downwind over rural areas. The warm plume over the cooler surface layer in the rural regions is associated with a shallow stable layer just downwind of the densest urban area, which deepens further downwind.

In stark contrast to BouLac, the MYJ configurations exhibit a deep stable layer from the sur-

face up to 400 m upwind of the city. Runs with SLUCM and BEP demonstrated little change over the city with slightly lower lapse rates. Given such a strong stability upwind of the city, mixing would be suppressed unless ample surface fluxes could contribute. Only the MYJ simulations that included the BEP+BEM UCM exhibited significant changes to the lower atmospheric stability. Using all of the different metrics to assess model performance over the Dallas-Fort Worth region during this period, the BEP+BEM and MYJ pairing tends to be the most representative in regards to temperature near the urban center and the lowest 500m of the atmosphere, which is critical when determining the low-level stability.

The urban environment is a complex region with many processes occurring at disparate spatial and temporal scales. Results from this work emphasize the importance of not just the UCM in correctly simulated the urban environment, but also the PBL scheme when simulating the atmosphere over urban areas. In fact, the sensitivity of the model output to PBL dominated over the sensitivity to the UCM. The bias in surface temperature and the stability in the lower atmosphere attributed to the PBL has important consequences to how the UHI and near-surface pollution is represented in models.

References

1. Arnfield, A. J. Two decades of urban climate research: a review of turbulence, exchanges of energy and water, and the urban heat island. *International Journal of Climatology* **23,** 1–26 (2003).

2. Arya, S. *Introduction to Micrometeorology. Second Edition* (Academic Press, 2001).

3. Baklanov, A. The Mixing Height in Urban Areas-a Review (Jan. 2002).

4. Barlow, J. Progress in observing and modelling the urban boundary layer. *Urban Climate* **10** (Aug. 2014).

5. Bougeault, P. & Lacarrere, P. Parameterization of Orography-Induced Turbulence in a Mesobeta–Scale Model. *Monthly Weather Review* **117,** 1872–1890. eprint: https://doi.org/10.1175/1520-0493(1989)117<1872:POOITI>2.0.CO;2. https://doi.org/10.1175/1520-0493(1989)117<1872:POOITI>2.0.CO;2 (1989).

6. Changnon, S. A., Huff, F. A. & Semonin, R. G. METROMEX: An investigation of inadvertent weather modification. *Bulletin of the American Meteorological Society* **52,** 958–968 (1971).

7. Clarke, J. F. NOCTURNAL URBAN BOUNDARY LAYER OVER CINCINNATI, OHIO. *Monthly Weather Review* **97,** 582–589. eprint: https://doi.org/10.1175/1520-0493(1969)097<0582:NUBLOC>2.3.CO;2. https://doi.org/10.1175/1520-0493(1969)097<0582:NUBLOC>2.3.CO;2 (1969).

8. Cosgrove, A. & Berkelhammer, M. Downwind footprint of an urban heat island on air and lake temperatures. *npj Climate and Atmospheric Science* **1** (Dec. 2018).

9. Deardorff, J. W. Theoretical expression for the countergradient vertical heat flux. *Journal of Geophysical Research (1896-1977)* **77,** 5900–5904. eprint: https://agupubs.onlinelibrary.wiley.com/doi/pdf/10.1029/JC077i030p05900. https://agupubs.onlinelibrary.wiley.com/doi/abs/10.1029/JC077i030p05900 (1972).

10. Frumkin, H. Urban sprawl and public health. *Public Health Reports* **117,** 201–217 (2002).

11. Glotfelty, T. *et al.* NUDAPT 44 Documentation (2013).

12. Godowitch, J. M., Ching, J. K. S. & Clarke, J. F. Evolution of the Nocturnal Inversion Layer at an Urban and Nonurban Location. *Journal of Climate and Applied Meteorology* **24,** 791–804. eprint: https://doi.org/10.1175/1520-0450(1985)024<0791:EOTNIL>2.0.CO;2. https://doi.org/10.1175/1520-0450(1985)024<0791:EOTNIL>2.0.CO;2 (1985).

13. Harnack, R. P. & Landsberg, H. Selected cases of convective precipitation caused by the metropolitan area of Washington, DC. *Journal of Applied Meteorology* **14,** 1050–1060 (1975).

14. Hong, S.-Y., Dudhia, J. & Chen, S.-H. A Revised Approach to Ice Microphysical Processes for the Bulk Parameterization of Clouds and Precipitation. *Monthly Weather Review* **132,** 103–120. eprint: https://doi.org/10.1175/1520-0493(2004)132<0103:ARATIM>2.0.CO;2. https://doi.org/10.1175/1520-0493(2004)132<0103:ARATIM>2.0.CO;2 (2004).

15. Iacono, M. J. *et al.* Radiative forcing by long-lived greenhouse gases: Calculations with the AER radiative transfer models. *Journal of Geophysical Research: Atmospheres* **113.** eprint: https://agupubs.onlinelibrary.wiley.com/doi/pdf/10.1029/2008JD009944. https://agupubs.onlinelibrary.wiley.com/doi/abs/10.1029/2008JD009944 (2008).

16. Janjić, Z. I. The Step-Mountain Coordinate: Physical Package. *Monthly Weather Review* **118,** 1429–1443. eprint: https://doi.org/10.1175/1520-0493(1990)118<1429:TSMCPP>2.0.CO;2. https://doi.org/10.1175/1520-0493(1990)118<1429:TSMCPP>2.0.CO;2 (1990).

17. Kain, J. S. & Fritsch, J. M. in *The Representation of Cumulus Convection in Numerical Models* (eds Emanuel, K. A. & Raymond, D. J.) 165–170 (American Meteorological Society, Boston, MA, 1993). ISBN: 978-1-935704-13-3. https://doi.org/10.1007/978-1-935704-13-3_16.

18. Kusaka, H., Kondo, H., Kikegawa, Y. & Kimura, F. A Simple Single-Layer Urban Canopy Model For Atmospheric Models: Comparison With Multi-Layer And Slab Models. *Boundary-Layer Meteorology* **101,** 329–358. ISSN: 1573-1472. https://doi.org/10.1023/A:1019207923078 (2001).

19. LeMone, M. A., Tewari, M., Chen, F. & Dudhia, J. Objectively Determined Fair-Weather CBL Depths in the ARW-WRF Model and Their Comparison to CASES-97 Observations. *Monthly Weather Review* **141,** 30–54. ISSN: 0027-0644. eprint: https://journals.ametsoc.org/mwr/article-pdf/141/1/30/4283977/mwr-d-12-00106_1.pdf. https://doi.org/10.1175/MWR-D-12-00106.1 (Jan. 2013).

20. Lumley, J. & Khajeh-Nouri, B. Modeling Homogenous Deformation of Turbulence. *Advanced Geophysics* **18A,** 162–192 (1974).

21. Mellor, G. L. & Yamada, T. Development of a turbulence closure model for geophysical fluid problems. *Reviews of Geophysics* **20,** 851–875. eprint: https://agupubs.onlinelibrary.wiley.com/doi/pdf/10.1029/RG020i004p00851. https://agupubs.onlinelibrary.wiley.com/doi/abs/10.1029/RG020i004p00851 (1982).

22. Murage, P., Hajat, S. & Kovats, R. S. Effect of night-time temperatures on cause and age-specific mortality in London. *Environmental Epidemiology* **1,** e005 (2017).

23. Niu, G.-Y. *et al.* The community Noah land surface model with multiparameterization options (Noah-MP): 1. Model description and evaluation with local-scale measurements. *Journal of Geophysical Research: Atmospheres* **116.** eprint: https://agupubs.onlinelibrary.wiley.com/doi/pdf/10.1029/2010JD015139. https://agupubs.onlinelibrary.wiley.com/doi/abs/10.1029/2010JD015139 (2011).

24. O'Brien, J. J. A Note on the Vertical Structure of the Eddy Exchange Coefficient in the Planetary Boundary Layer. *Journal of the Atmospheric Sciences* **27,** 1213–1215. eprint: https://doi.org/10.1175/1520-0469(1970)027<1213:ANOTVS>2.0.CO;2. https://doi.org/10.1175/1520-0469(1970)027<1213:ANOTVS>2.0.CO;2 (1970).

25. Oke, T. The urban energy balance. *Progress in Physical Geography: Earth and Environment* **12,** 471–508. eprint: https://doi.org/10.1177/030913338801200401. https://doi.org/10.1177/030913338801200401 (1988).

26. Rahn, D. A. & Mitchell, C. J. Diurnal Climatology of the Boundary Layer in Southern California Using AMDAR Temperature and Wind Profiles. *Journal of Applied Meteorology and Climatology* **55,** 1123–1137. eprint: https://doi.org/10.1175/JAMC-D-15-0234.1. https://doi.org/10.1175/JAMC-D-15-0234.1 (2016).

27. Rizwan, A. M., Dennis, L. Y. & Liu, C. A review on the generation, determination and mitigation of Urban Heat Island. *Journal of Environmental Sciences* **20,** 120 –128. ISSN: 1001-0742. http://www.sciencedirect.com/science/article/pii/S1001074208600194 (2008).

28. Salamanca, F., Georgescu, M., Mahalov, A, Moustaoui, M & Wang, M. Anthropogenic heating of the urban environment due to air conditioning. *Journal of Geophysical Research: Atmospheres* **119,** 5949–5965 (2014).

29. Salamanca, F. & Martilli, A. A new Building Energy Model coupled with an Urban Canopy Parameterization for urban climate simulations—part II. Validation with one dimension off-line simulations. *Theoretical and Applied Climatology* **99,** 345. ISSN: 1434-4483. https://doi.org/10.1007/s00704-009-0143-8 (2009).

30. Salamanca, F., Martilli, A., Tewari, M. & Chen, F. A Study of the Urban Boundary Layer Using Different Urban Parameterizations and High-Resolution Urban Canopy Parameters with WRF. *Journal of Applied Meteorology and Climatology* **50,** 1107–1128. eprint: https://doi.org/10.1175/2010JAMC2538.1. https://doi.org/10.1175/2010JAMC2538.1 (2011).

31. Seidel, D. J. *et al.* Climatology of the planetary boundary layer over the continental United States and Europe. *Journal of Geophysical Research: Atmospheres* **117.** eprint: https://

agupubs . onlinelibrary . wiley . com / doi / pdf / 10 . 1029 / 2012JD018143. https : //agupubs.onlinelibrary.wiley.com/doi/abs/10.1029/2012JD018143 (2012).

32. Shahmohamadi, P, Che-Ani, A., Maulud, K., Tawil, N. & Abdullah, N. The impact of anthropogenic heat on formation of urban heat island and energy consumption balance. *Urban Studies Research* **2011** (2011).

33. Sharma, A. *et al.* Urban meteorological modeling using WRF: a sensitivity study. *International Journal of Climatology* **37,** 1885–1900. eprint: https : //rmets . onlinelibrary . wiley . com/doi/pdf/10 . 1002/joc . 4819. https : //rmets . onlinelibrary . wiley . com/doi/abs/10.1002/joc.4819 (2017).

34. Skamarock, W. C. *et al. A Description of the Advanced Research WRF Model Version 4* en. Tech. rep. (2019).

35. Sobrino, J. A. *et al.* Evaluation of the surface urban heat island effect in the city of Madrid by thermal remote sensing. *International journal of remote sensing* **34,** 3177–3192 (2013).

36. Wood, C. R. *et al.* An Overview of the Urban Boundary Layer Atmosphere Network in Helsinki. *Bulletin of the American Meteorological Society* **94,** 1675–1690. eprint: https : //doi.org/10.1175/BAMS-D-12-00146.1. https://doi.org/10.1175/BAMS-D-12-00146.1 (2013).

37. Zhao, L., Lee, X., B Smith, R. & Oleson, K. Strong contribution of local background climate to urban heat islands. *Nature* **511,** 216–9 (July 2014).